



1 **Modeling of the chemistry in oxidation flow reactors with high initial NO**

2 Zhe Peng<sup>1,2</sup> and Jose L. Jimenez<sup>1,2</sup>

3 <sup>1</sup> Cooperative Institute for Research in Environmental Sciences, University of Colorado, Boulder, CO 80309, USA

4 <sup>2</sup> Department of Chemistry and Biochemistry, University of Colorado, Boulder, CO 80309, USA

5 Correspondence to: J.L. Jimenez (jose.jimenez@colorado.edu)

6

7 **Abstract.** Oxidation flow reactors (OFRs) are increasingly employed in atmospheric chemistry research  
8 because of their high efficiency of OH radical production from low-pressure Hg lamp emissions at both  
9 185 and 254 nm (OFR185) or 254 nm only (OFR254). OFRs have been thought to be limited to studying  
10 low-NO chemistry (where peroxy radicals (RO<sub>2</sub>) react preferentially with HO<sub>2</sub>) because NO is very rapidly  
11 oxidized by the high concentrations of O<sub>3</sub>, HO<sub>2</sub>, and OH in OFRs. However, many groups are performing  
12 experiments aging combustion exhaust with high NO levels, or adding NO in the hopes of simulating  
13 high-NO chemistry (where RO<sub>2</sub> + NO dominates). This work systematically explores the chemistry in  
14 OFRs with high initial NO. Using box modeling, we investigate the interconversion of N-containing  
15 species and the uncertainties due to kinetic parameters. Simple initial injection of NO in OFR185 can  
16 result in more RO<sub>2</sub> reacted with NO than with HO<sub>2</sub> and minor non-tropospheric photolysis, but only  
17 under a very narrow set of conditions (high water mixing ratio, low UV intensity, low external OH  
18 reactivity (OHR<sub>ext</sub>), and initial NO concentration (NO<sup>in</sup>) of tens to hundreds of ppb) that account for a  
19 very small fraction of the input parameter space. These conditions are generally far away from  
20 experimental conditions of published OFR studies with high initial NO. In particular, studies of aerosol  
21 formation from vehicle emissions in OFR often used OHR<sub>ext</sub> and NO<sup>in</sup> several orders of magnitude higher.  
22 Due to extremely high OHR<sub>ext</sub> and NO<sup>in</sup>, some studies may have resulted in substantial non-tropospheric  
23 photolysis, strong delay to RO<sub>2</sub> chemistry due to peroxyxynitrate formation, VOC reactions with NO<sub>3</sub>  
24 dominating over those with OH, and faster reactions of OH-aromatic adducts with NO<sub>2</sub> than those with  
25 O<sub>2</sub>, all of which are irrelevant to ambient VOC photooxidation chemistry. Some of the negative effects  
26 are worst for alkene and aromatic precursors. To avoid undesired chemistry, vehicle emissions generally  
27 need to be diluted by a factor of >100 before being injected into OFR. However, sufficiently diluted  
28 vehicle emissions generally do not lead to high-NO chemistry in OFR, but are rather dominated by the  
29 low-NO RO<sub>2</sub>+HO<sub>2</sub> pathway. To ensure high-NO conditions without substantial atmospherically irrelevant  
30 chemistry in a more controlled fashion, new techniques are needed.



## 31 1 Introduction

32 The oxidation of gases that are emitted into the atmosphere, in particular volatile organic  
33 compounds (VOCs), is one of the most important atmospheric chemistry processes (Haagen-Smit, 1952;  
34 Chameides et al., 1988). VOC oxidation is closely related to radical production and consumption (Levy  
35 II, 1971), O<sub>3</sub> production, and formation of secondary aerosols (Odum et al., 1996; Hoffmann et al., 1997;  
36 Volkamer et al., 2006; Hallquist et al., 2009), which have impacts on air quality and climate (Lippmann,  
37 1991; Nel, 2005; Stocker et al., 2014).

38 Chemical reactors are critical tools for research of VOC oxidation. Oxidation reactions of interest  
39 often have typical timescales of hours to weeks. Studying these processes in ambient air can be  
40 confounded by dispersion and changes in ambient conditions, which often occur in similar timescales.  
41 Chemical reactors allow for decoupling these two types of processes. Also, they should be able to  
42 simulate the different regimes of reactions occurring in the atmosphere, e.g., VOC oxidation under low  
43 and high-NO conditions (peroxy radical fate dominated by reaction with HO<sub>2</sub> or with NO) representing  
44 remote and urban areas, respectively (Orlando and Tyndall, 2012).

45 Large environmental chambers are a commonly used reactor type (Carter et al., 2005; Wang et al.,  
46 2011). They typically employ actinic wavelength (>300 nm) light sources (e.g., outdoor solar radiation  
47 and UV blacklights) to produce oxidants and radicals and have large volumes (on the order of several  
48 cubic meters or larger). However, the capability of generating sustained elevated levels of OH, the most  
49 important tropospheric oxidant, is usually limited in chambers, resulting in OH concentrations similar  
50 to those in the atmosphere (10<sup>6</sup>–10<sup>7</sup> molecules cm<sup>-3</sup>; Mao et al., 2009; Ng et al., 2010), and consequently,  
51 long simulation times (typically hours) to reach OH equivalent ages of atmospheric relevance (George  
52 et al., 2007; Kang et al., 2007; Carlton et al., 2009; Seakins, 2010; Wang et al., 2011). The partitioning of  
53 gases and aerosols to chamber walls (usually made of Teflon) in timescales of tens of minutes to hours  
54 makes it difficult to conduct very long experiments that simulate high atmospherically-relevant  
55 photochemical ages (Cocker et al., 2001; Matsunaga and Ziemann, 2010; Zhang et al., 2014; Krechmer  
56 et al., 2016). In addition, the long simulation times and large size of chambers and auxiliary equipment  
57 are logistically difficult for field deployment, and their cost limits the number of laboratories equipped  
58 with them.

59 Given the limitations of environmental chambers, a growing number of experimenters have  
60 instead employed oxidation flow reactors (OFRs). OFRs have a much smaller size (of the order of 10 L),  
61 efficiently generate OH via photolysis of H<sub>2</sub>O and/or O<sub>3</sub> by more energetic 185 and 254 nm photons  
62 from low-pressure Hg lamps, and overcome the abovementioned shortcomings of chambers due to a  
63 much shorter residence time (George et al., 2007; Kang et al., 2007, 2011; Lambe et al., 2011). Moreover,  
64 OFRs are able to rapidly explore a wide range of OH equivalent ages within a short period (~2 hr), during  
65 which significant changes of ambient conditions can usually be avoided in the case of field deployment  
66 (Ortega et al., 2016; Palm et al., 2016, 2017). Because of these advantages, OFRs have recently been  
67 widely used to study atmospheric chemistry, in particular secondary organic aerosol (SOA) formation  
68 and aging, in both the laboratory and the field (Kang et al., 2011; Li et al., 2013; Ortega et al., 2013,



69 2016; Tkacik et al., 2014; Palm et al., 2016).

70 In addition to experimental studies using OFRs, there has also been some progress in the  
71 characterization of OFR chemistry by modeling. Li et al. (2015) and Peng et al. (2015) developed a box  
72 model for OFR HO<sub>x</sub> chemistry that predicts measurable quantities [e.g., OH exposure (OH<sub>exp</sub>) and O<sub>3</sub>  
73 concentration (abbr. O<sub>3</sub> hereinafter)] in good agreement with experiments. This model has been used  
74 to characterize HO<sub>x</sub> chemistry as a function of H<sub>2</sub>O mixing ratio (abbr. H<sub>2</sub>O hereinafter), UV light intensity  
75 (abbr. UV hereinafter), and external OH reactivity [OHR<sub>ext</sub>=∑k<sub>i</sub>C<sub>i</sub>, i.e., the sum of the products of  
76 concentrations of externally introduced OH-consuming species (c<sub>i</sub>) and rate constants of their reactions  
77 with OH (k<sub>i</sub>). Based on this characterization, Peng et al. (2015) found that OH suppression, i.e.,  
78 reduction of OH concentration caused by OHR<sub>ext</sub>, is a common feature under many typical OFR operation  
79 conditions. Peng et al. (2016) systematically examined the relative importance of non-OH/non-  
80 tropospheric reactants on the fate of VOCs over a wide range of conditions, and provided guidelines for  
81 OFR operation to avoid non-tropospheric reactions.

82 In previous OFR modeling studies, NO<sub>x</sub> chemistry was not investigated in detail, since in such in  
83 typical OFR experiments with large amounts of oxidants (e.g., OH, HO<sub>2</sub>, and O<sub>3</sub>), NO would be very  
84 rapidly oxidized and thus unable to compete with HO<sub>2</sub> for reaction with peroxy radicals (RO<sub>2</sub>). Li et al.  
85 (2015) estimated an NO (NO<sub>2</sub>) lifetime of ~0.5 (~1.5) s under a typical OFR condition. From these  
86 estimates, OFRs processing ambient air or laboratory air without large addition of NO<sub>x</sub> were assumed  
87 to be not suitable for studying oxidation mechanisms relevant to polluted conditions under higher NO  
88 concentrations. OFRs have recently been used to conduct laboratory experiments with very high initial  
89 NO<sub>x</sub> levels (Liu et al., 2015) and deployed to an urban tunnel, where NO<sub>x</sub> was high enough to be a major  
90 OH reactant (Tkacik et al., 2014). The former study reported evidence for the incorporation of nitrogen  
91 into SOA. Besides, OFRs have been increasingly employed to process emissions of vehicles, biomass  
92 burning, and other combustion sources (Table 1), where NO can often be hundreds of ppm (Ortega et  
93 al., 2013; Martinsson et al., 2015; Karjalainen et al., 2016; Link et al., 2016; Schill et al., 2016; Simonen  
94 et al., 2016; Alanen et al., 2017). It can be expected that such a high NO input together with very high  
95 VOC concentrations would cause a substantial deviation from good OFR operation conditions identified  
96 in Peng et al. (2016). Very recently, N<sub>2</sub>O injection has been proposed by Lambe et al. (2017) as a way to  
97 study oxidation of VOCs under high NO conditions in OFR. As more OFR studies at high NO<sub>x</sub> level are  
98 conducted, there is growing need to understand the chemistry of N-containing species in OFRs and  
99 whether it proceeds along atmospherically-relevant channels.

100 In this study, we present the first comprehensive model of OFR NO<sub>y</sub> chemistry. We extend the  
101 model of Li et al. (2015) and Peng et al. (2015) by including a scheme for NO<sub>y</sub> species. Then this model  
102 is used to investigate i) if an OFR with initial NO injection results in NO significantly reacting with RO<sub>2</sub>  
103 under any conditions, ii) if previously published OFR experiments with high initial NO concentrations  
104 led to RO<sub>2</sub>+NO being dominant in VOC oxidation without negative side effects (e.g., non-tropospheric  
105 reactions), iii) how to avoid undesired chemistry in future studies. The results can provide insights into  
106 the design and interpretation of future OH-oxidation OFR experiments with large amounts of NO<sub>x</sub>



107 injection.

## 108 **2 Methods**

109 The physical design of the OFR modeled in the present work, the chemical kinetics box model, and  
110 the method of propagating and analyzing the parametric uncertainties on the model have already been  
111 introduced previously (Kang et al., 2007; Li et al., 2015; Peng et al., 2015). We only provide brief  
112 descriptions for them below.

### 113 **2.1 Potential Aerosol Mass flow reactor**

114 The OFR modeled in this study is the “Potential Aerosol Mass” (PAM) flow reactor, firstly  
115 introduced by Kang et al. (2007). The PAM OFR is a cylindrical vessel with a volume of ~13 L, equipped  
116 with low-pressure Hg lamps (model no. 82-9304-03, BHK Inc.) to generate 185 and 254 nm UV light.  
117 This popular design is being used by many atmospheric chemistry research groups, particularly those  
118 studying SOA (Lambe and Jimenez, 2017 and references therein). When the lamps are mounted inside  
119 Teflon sleeves, photons at both wavelengths are transmitted and contribute to OH production (“OFR185  
120 mode”). In OFR185, H<sub>2</sub>O photolyzed at 185 nm produces OH and HO<sub>2</sub>, while O<sub>2</sub> photolyzed at the same  
121 wavelengths results in O<sub>3</sub> formation. O(<sup>1</sup>D) is produced via O<sub>3</sub> photolysis at 254 nm and generates  
122 additional OH through its reaction with H<sub>2</sub>O. 185 nm lamp emissions can be filtered by mounting the  
123 lamps inside quartz sleeves, leaving only 254 nm photons to produce OH (“OFR254 mode”). In this mode,  
124 injection of externally formed O<sub>3</sub> is necessary to ensure OH production. As the amount of O<sub>3</sub> injected is  
125 a key parameter under some conditions (Peng et al., 2015), we adopt the notation OFR254-X to denote  
126 OFR254 experiments with X ppm initial O<sub>3</sub> (O<sub>3,in</sub>). In this study, we investigate OFR experiments with NO  
127 injected and thus utilize “OFR185-iNO” to describe the OFR185 mode of operation with initially (at the  
128 reactor entrance) injected NO. The same terminology is used for the OFR254 mode. For instance, the  
129 initial NO injection into OFR254-7 is denoted as OFR254-7-iNO.

### 130 **2.2 Model description**

131 The basic framework of the box model used in this study, a standard chemical kinetics model, is  
132 the same as in Peng et al. (2015). Plug flow is assumed in the model, since approximately taking  
133 residence time distribution into account leads to similar results under most conditions but at much  
134 higher computational expense (Peng et al., 2015). In addition to the reactions in the model of Peng et  
135 al. (2015), including all HO<sub>x</sub> reactions available in the JPL Chemical Kinetic Data Evaluation (Sander et al.,  
136 2011), all gas-phase NO<sub>y</sub> reactions available in the JPL database except those of organic nitrates and  
137 peroxy nitrates are also considered in the current reaction scheme. An updated JPL evaluation was  
138 published recently (Burkholder et al., 2015), with slightly different (~20%) rate constants for  
139 NO<sub>2</sub>+HO<sub>2</sub>+M→HO<sub>2</sub>NO<sub>2</sub>+M and NO<sub>2</sub>+NO<sub>3</sub>→N<sub>2</sub>O<sub>5</sub>. The updated rate constants only result in changes of  
140 ~10–20% of the concentrations of the species directly consumed/produced by these reactions. These  
141 changes are smaller than the parametric uncertainties of the model (see Section 3.1.3). For other  
142 species, concentration changes are negligible. HO<sub>2</sub>NO<sub>2</sub>+M→HO<sub>2</sub>+NO<sub>2</sub>+M and N<sub>2</sub>O<sub>5</sub>+M→NO<sub>2</sub>+NO<sub>3</sub>+M,  
143 are also included in the scheme, with kinetic parameters from the IUPAC Task Group on Atmospheric  
144 Chemical Kinetic Data Evaluation (Ammann et al., 2016). As in Peng et al. (2015, 2016), SO<sub>2</sub> is used as a



145 surrogate of external OH reactants (e.g., VOCs). NO<sub>y</sub> species, although also external OH reactants, are  
146 explicitly treated in the model and *not* counted in OHR<sub>ext</sub> in this work. Therefore, OHR<sub>ext</sub> stands for *non*-  
147 NO<sub>y</sub> OHR<sub>ext</sub> only hereinafter, unless otherwise stated.

148 A residence time of 180 s and typical temperature (295 K) and atmospheric pressure (835 mbar)  
149 in Boulder, CO, USA are assumed for all model cases. The lower-than-sea level pressure only leads to  
150 minor differences in the outputs (Li et al., 2015). We explore physical input cases evenly spaced in a  
151 logarithmic scale over very wide ranges: H<sub>2</sub>O of 0.07%–2.3%, i.e., relative humidity (RH) of 2–71% at  
152 295 K; 185 nm UV of 1.0x10<sup>11</sup>–1.0x10<sup>14</sup> and 254 nm UV of 4.2x10<sup>13</sup>–8.5x10<sup>15</sup> photons cm<sup>-2</sup> s<sup>-1</sup>; OHR<sub>ext</sub> of  
153 1–16000 s<sup>-1</sup>; O<sub>3,in</sub> of 2.2–70 ppm for OFR254; initial NO mixing ratio (NO<sup>in</sup>) from 10 ppt to 40 ppm.  
154 Besides, conditions with OHR<sub>ext</sub>=0 are also explored. UV at 254 nm is estimated from that at 185 nm  
155 according to the relationship determined by Li et al. (2015). Several typical cases within this range are  
156 defined in Table 2. Literature studies are modeled by adopting all reported parameters (e.g., residence  
157 time, H<sub>2</sub>O, and O<sub>3,in</sub>) and estimating any others that may be needed (e.g., UV) from the information  
158 provided in the papers.

159 In this study, OH equivalent ages are calculated under the assumption of an ambient OH  
160 concentration of 1.5x10<sup>5</sup> molecules cm<sup>-3</sup> (Mao et al., 2009). Conditions leading to a ratio of RO<sub>2</sub> reacted  
161 with NO over the entire residence time [r(RO<sub>2</sub>+NO)] to that with HO<sub>2</sub> [r(RO<sub>2</sub>+HO<sub>2</sub>)] larger than 1 are  
162 regarded as “high NO” (under the assumption of constant OHR<sub>ext</sub> from VOCs, see Section S1 for more  
163 details), where [r(X)] is the total reactive flux for reaction X over the entire residence time. F<sub>185<sub>exp</sub></sub>/OH<sub>exp</sub>  
164 and F<sub>254<sub>exp</sub></sub>/OH<sub>exp</sub> are used as measures of the relative importance of VOC photolysis at 185 and 254  
165 nm to their reactions with OH, respectively [F<sub>185<sub>exp</sub></sub> (F<sub>254<sub>exp</sub></sub>) are 185 (254) nm photon flux exposure,  
166 i.e., product of 185 (254) nm photon flux and time]. Readers may refer to Figs. 1 and 2 of Peng et al.  
167 (2016) for the determination of the relative importance of non-tropospheric (185 and 254 nm)  
168 photolysis of individual VOCs. Although the relative importance of non-tropospheric photolysis depends  
169 on individual VOCs, in the present work, we set criteria on F<sub>185<sub>exp</sub></sub>/OH<sub>exp</sub><3x10<sup>3</sup> cm/s and  
170 F<sub>254<sub>exp</sub></sub>/OH<sub>exp</sub><4x10<sup>5</sup> cm/s to define “good” conditions and F<sub>185<sub>exp</sub></sub>/OH<sub>exp</sub><1x10<sup>5</sup> cm/s and  
171 F<sub>254<sub>exp</sub></sub>/OH<sub>exp</sub><1x10<sup>7</sup> cm/s (excluding good conditions) to define “risky” conditions. Conditions with  
172 higher F<sub>185<sub>exp</sub></sub>/OH<sub>exp</sub> or F<sub>254<sub>exp</sub></sub>/OH<sub>exp</sub> are defined as “bad”. Under good conditions, photolysis of most  
173 VOCs has a relative contribution <20% to their fate. Under risky conditions, some species photolyzing  
174 slowly and/or reacting with OH rapidly (e.g., alkanes, aldehydes, and most biogenics) still have a relative  
175 contribution of photolysis <20% to their fates, while species photolyzing more rapidly and/or reacting  
176 with OH more slowly (e.g., aromatics and other highly conjugated species and some saturated carbonyls)  
177 risk substantial non-tropospheric photolysis. Note that these definitions are slightly different than in  
178 Peng et al. (2016). All definitions of the types of conditions are summarized in Table 3.

### 179 2.3 Uncertainty analysis

180 We apply the same method as in Peng et al. (2014, 2015) to calculate and analyze the output  
181 uncertainties due to uncertain kinetic parameters in the model. Random samples following log-normal  
182 distributions are generated for all rate constants and photoabsorption cross sections in the model using



183 uncertainty data available in the JPL database (Sander et al., 2011) or estimated based on IUPAC data  
184 (Ammann et al., 2016). Then, Monte Carlo Uncertainty Propagation (BIPM et al., 2008) is performed for  
185 these samples through the model to obtain the distributions of outputs. Finally, we compute squared  
186 correlation coefficients between corresponding input and output samples and apportion the relative  
187 contributions of individual kinetic parameters to the output uncertainties based on these coefficients  
188 (Saltelli et al., 2005).

### 189 **3 Results and discussion**

190 In this section, we study the  $\text{NO}_y$  chemistry in OFR while considering relevant experimental issues.  
191 Based on these results, we propose some guidelines for OFR operation for high-NO OH oxidation of  
192 VOCs.

#### 193 **3.1 $\text{NO}_y$ chemistry in typical OFR cases with initial NO injection**

194 NO was thought to be unimportant (i.e., unable to significantly react with  $\text{RO}_2$ ) in OFRs with initial  
195 NO injection (OFR-iNO) based on the argument that its lifetime is too short due to large amounts of  $\text{O}_3$   
196 OH, and  $\text{HO}_2$  to compete with  $\text{RO}_2+\text{HO}_2$  (Li et al., 2015). We evaluate this issue below by calculating NO  
197 effective lifetime ( $\tau_{\text{NO}}$ ), defined as NO exposure ( $\text{NO}_{\text{exp}}$ ) divided by initial NO concentration, under  
198 various conditions. This definition cannot effectively capture the true NO average lifetime if it is close  
199 to or longer than the residence time. In this case,  $\tau_{\text{NO}}$  close to the residence time will be obtained, which  
200 is still long enough for our characterization purposes.

##### 201 **3.1.1 OFR185-iNO**

202 In OFR185-iNO, NO is *not* oxidized extremely quickly under *all* conditions. For instance, under a  
203 typical condition in the midrange of the phase space shown in Fig. 1a,  $\tau_{\text{NO}} \sim 13$  s. This lifetime is much  
204 shorter than the residence time, but long enough to suppress  $\text{HO}_2$  through the reaction  
205  $\text{NO}+\text{HO}_2 \rightarrow \text{NO}_2+\text{OH}$ , leading to  $\text{NO}_{\text{exp}}/\text{HO}_{2\text{exp}}$  of  $\sim 700$  during this period, high enough for  $\text{RO}_2$   
206 to dominantly react with NO. Meanwhile,  $\text{NO}+\text{HO}_2 \rightarrow \text{NO}_2+\text{OH}$  enhances OH production. Within  $\tau_{\text{NO}}$ ,  $\text{OH}_{\text{exp}}$   
207 reaches  $\sim 3 \times 10^{10}$  molecules  $\text{cm}^{-3}$  s, which is equivalent to an OH equivalent age of  $\sim 6$  hrs. Such an OH  
208 equivalent age is already sufficient to allow some VOC processing and even SOA formation to occur  
209 (Lambe et al., 2011; Ortega et al., 2016). In addition, non-tropospheric photolysis of VOCs at 185 and  
210 254 nm is minor, because of enhanced OH production and moderate UV. Therefore, such an OFR  
211 condition may be of some interest for high-NO VOC oxidation. We thus analyze the  $\text{NO}_y$  chemistry in  
212 OFR185-iNO in more detail below, by taking the case shown in Fig. 1a as a representative example.

213 In OFR185-iNO,  $\text{HO}_x$  concentrations are orders-of-magnitude higher than in the atmosphere  
214 while the amount of  $\text{O}_3$  produced is relatively small during the first several seconds after the flow enters  
215 the reactor. As a result, NO is not oxidized almost exclusively by  $\text{O}_3$  as in the troposphere, but also by  
216 OH and  $\text{HO}_2$  to form HONO and  $\text{NO}_2$ , respectively (Fig. 1a). The large concentration of OH present then  
217 oxidizes HONO and  $\text{NO}_2$  to  $\text{NO}_2$  and  $\text{HNO}_3$ , respectively. Photolysis is the main atmospheric fate of HONO  
218 and  $\text{NO}_2$ , but photolysis proceeds to a much smaller extent (typically orders of magnitude smaller in  
219 terms of e-fold decay) in OFRs than in the troposphere at the same OH equivalent age (Peng et al., 2016).  
220 However, the interconversion between  $\text{NO}_2$  and  $\text{HO}_2\text{NO}_2$  is greatly accelerated (Fig. 1a), since a large



221 amount of HO<sub>2</sub> promotes the formation of HO<sub>2</sub>NO<sub>2</sub>, whose thermal decomposition and reaction with  
222 OH in turn enhance the recycling of NO<sub>2</sub>. Though not explicitly modeled in this study, RO<sub>2</sub> are expected  
223 to undergo similar reactions with NO<sub>2</sub> to form reservoir species, i.e., peroxy nitrates (Orlando and Tyndall,  
224 2012). Peroxy nitrates that decompose on timescales greater than OFR residence times may serve as  
225 permanent NO<sub>y</sub> sinks in OFRs (see Section 3.3.1).

226 Interestingly but not surprisingly, the NO<sub>y</sub> chemistry shown in Fig. 1a is far from temporally  
227 uniform during the OFR residence time (Fig. S1a). Within  $\tau_{NO}$ , NO undergoes an e-fold decay as it is  
228 rapidly converted into NO<sub>2</sub> and HONO, whose concentrations reach maxima around that time. After  
229 most NO is consumed, HONO and NO<sub>2</sub> also start to decrease, but significantly more slowly than NO,  
230 since they do not have as many and efficient loss pathways as NO. The reaction of OH with HONO, the  
231 dominant fate of HONO, is slower than that with NO. The net rate of the NO<sub>2</sub>-to-HO<sub>2</sub>NO<sub>2</sub> conversion  
232 becomes low because of the relatively fast reverse reaction. Besides, the total loss of NO<sub>2</sub> is partially  
233 offset by the production from HONO. The generally stable concentrations of HONO and NO<sub>2</sub> result in  
234 their respective reaction rates with OH that are comparable during and after  $\tau_{NO}$ , as OH variation is also  
235 relatively small during the entire residence time (Fig. S1b). However, the NO<sub>2</sub>-to-HO<sub>2</sub>NO<sub>2</sub> conversion  
236 after  $\tau_{NO}$  is much faster than during it, resulting from substantially decreased NO and HO<sub>2</sub> concomitantly  
237 increasing >1 order of magnitude after  $\tau_{NO}$  (Fig. S1b). HNO<sub>3</sub> and HO<sub>2</sub>NO<sub>2</sub>, which are substantially  
238 produced only after NO<sub>2</sub> is built up, have much higher concentrations later than within  $\tau_{NO}$ .

239 Under other OFR185-iNO conditions than in Fig. 1a, the major reactions interconverting NO<sub>y</sub>  
240 species are generally the same, although their relative importance may vary. At lower NO<sup>in</sup>, the  
241 perturbation of HO<sub>x</sub> chemistry caused by NO<sub>y</sub> species is smaller. Effects of NO<sup>in</sup> less than 1 ppb (e.g.,  
242 typical non-urban ambient concentrations) are generally negligible regarding HO<sub>x</sub> chemistry. Regarding  
243 NO<sub>y</sub> species, the pathways in Fig. 1a are still important under those conditions. At higher NO<sup>in</sup> (e.g., >1  
244 ppm), one might expect NO<sub>3</sub> and N<sub>2</sub>O<sub>5</sub> to play a role (as in OFR254-iNO; see Section 3.1.2 below), since  
245 high NO<sub>y</sub> concentrations might enhance self/cross reactions of NO<sub>y</sub>. However, this would not occur  
246 unless OH production is high, since relatively low O<sub>3</sub> concentrations in OFR185-iNO cannot oxidize NO<sub>2</sub>  
247 to NO<sub>3</sub> rapidly. Also, a large amount of NO<sub>y</sub> can lead to significant OH suppression. That would in turn  
248 slow down the NO<sub>3</sub> production from HNO<sub>3</sub> by OH. This is especially true when an OFR is used to oxidize  
249 the output of highly concentrated sources (e.g., from vehicle exhausts). When sources corresponding  
250 to OHR<sub>ext</sub> of thousands of s<sup>-1</sup> and NO<sup>in</sup> of tens of ppm are injected into OFR185 (Fig. 1b), they essentially  
251 inhibit active chemistry except NO consumption, as all subsequent products are much less abundant  
252 compared to remaining NO (Fig. S1c).

### 253 3.1.2 OFR254-iNO

254 The ppm-level O<sub>3,in</sub> used in the OFR254-iNO mode of operation has a strong impact on its NO<sub>y</sub>  
255 chemistry. An O<sub>3,in</sub> of 2.2 ppm (lowest in this study) is already enough to shorten  $\tau_{NO}$  to ~1 s, preventing  
256 NO from playing a role in the chemistry under most explored conditions. The reaction fluxes under a  
257 typical O<sub>3,in</sub> of 7 ppm are shown in Fig. 1c. A reactive flux from NO+O<sub>3</sub>→NO<sub>2</sub> makes the reaction of NO  
258 with other oxidants (OH, HO<sub>2</sub> etc.) negligible. The HNO<sub>3</sub> production pathway from NO<sub>2</sub> is similar to that



259 in OFR185-iNO. The interconversion between  $\text{NO}_2$  and  $\text{HO}_2\text{NO}_2$  is also fast over the residence time, and  
260 even faster than in OFR185-iNO during  $\tau_{\text{NO}}$ , since a high concentration of  $\text{O}_3$  also controls the OH- $\text{HO}_2$   
261 interconversion and makes  $\text{HO}_2$  more resilient against suppression due to high NO (Fig. S1f; Peng et al.,  
262 2015). A major difference in the  $\text{NO}_y$  chemistry in OFR254-iNO (Fig. 1c) compared to OFR185-iNO (Fig.  
263 1a) is significant  $\text{NO}_3/\text{N}_2\text{O}_5$  chemistry due to high  $\text{O}_3$  in OFR254-iNO, which accelerates the oxidation of  
264  $\text{NO}_2$  to  $\text{NO}_3$ . Interconversion between  $\text{NO}_2+\text{NO}_3$  and  $\text{N}_2\text{O}_5$  also occurs to a significant extent because of  
265 high  $\text{NO}_2$ . Under the conditions of Fig. 1c,  $\text{NO}_3$  can also be significantly consumed by  $\text{HO}_2$ . Unlike  
266 OFR185-iNO, OFR254-iNO can substantially form  $\text{NO}_3$  from  $\text{HNO}_3$  under conditions that are not on the  
267 extremes of the explored physical condition space, e.g., at higher UV and lower  $\text{NO}^{\text{in}}$  (e.g., Fig. S2). In  
268 the case of very high  $\text{NO}^{\text{in}}$  (equal to or higher than  $\text{O}_{3,\text{in}}$ ), all  $\text{O}_3$  can be rapidly destroyed by NO. As a  
269 consequence, OH production is shut down and these cases are of little practical interest.

### 270 3.1.3 Uncertainty analysis

271 The results of uncertainty propagation confirm that the output uncertainties due to uncertain  
272 kinetic parameters are relatively low compared to other factors (e.g., non-plug flow in OFR; Peng et al.,  
273 2015) and the overall model accuracy compared to experimental data (a factor of 2–3; Li et al., 2015).  
274 For OFR185-iNO, NO,  $\text{NO}_3$ , and OH exposures have relative uncertainties of ~0–20%, ~40–70%, and ~15–  
275 40%, respectively. The uncertainties in OH exposure are very similar with those in the cases without  $\text{NO}_x$   
276 (Peng et al., 2015). The contribution of  $\text{NO}_y$  reactions to  $\text{OH}_{\text{exp}}$  uncertainty is negligible, except for some  
277 contribution of  $\text{OH}+\text{NO}\rightarrow\text{HONO}$  in a few cases with high  $\text{NO}^{\text{in}}$  (Fig. 2). The uncertainties on  $\text{NO}_{\text{exp}}$  are  
278 dominated by the reactions producing  $\text{HO}_x$  and  $\text{O}_3$ , i.e., the major consumers of NO. For  $\text{NO}_3$  exposure,  
279 a few major production and loss pathways (e.g.,  $\text{NO}_2+\text{NO}_3\rightarrow\text{N}_2\text{O}_5$ ,  $\text{N}_2\text{O}_5\rightarrow\text{NO}_2+\text{NO}_3$ , and  
280  $\text{HO}_2+\text{NO}_3\rightarrow\text{OH}+\text{NO}_2+\text{O}_2$ ) dominate its uncertainties. OFR254-iNO has a simpler picture of parametric  
281 uncertainties in terms of composition.  $\text{O}_3$  controls the NO oxidation under most conditions and this  
282 reaction contributes most of output uncertainties for NO exposures.  $\text{HO}_2+\text{NO}_3\rightarrow\text{OH}+\text{NO}_2+\text{O}_2$  dominates  
283 the uncertainty on  $\text{NO}_3$  exposure. The levels of those uncertainties are lower than in OFR185-iNO (<2%  
284 for NO exposure; <60% in all cases and <25% in most cases for  $\text{NO}_3$  exposure). Thus, model uncertainties  
285 in OFR254-iNO are not shown in detail.

### 286 3.2 Different conditions types

287 Having illustrated the main  $\text{NO}_y$  chemical pathways for typical cases, we present the results of  
288 the exploration of the entire physical parameter space (see Section 2.2). Note that the explored space  
289 is indeed very large and gridded logarithmically uniformly in every dimension. Therefore, the statistics  
290 of the exploration results can be useful to determine of the relative importance of the conditions types  
291 defined in Section 2.2 and Table 3.

292 It has been shown that during  $\tau_{\text{NO}}$ ,  $\text{RO}_2$  can react dominantly with NO (Section 3.1.1), while to  
293 determine if a condition is high-NO (see Table 3), the entire residence time is considered. This is done  
294 because for VOC oxidation systems of interest, there will be significant oxidation of the initial VOC and  
295 its products under low-NO conditions, if  $\tau_{\text{NO}}$  is shorter than the reactor residence time. After most NO  
296 is consumed, the longer the remaining residence time, the more  $\text{RO}_2$  will react with  $\text{HO}_2$  and the more





297 likely that an input condition is classified as low-NO. For a condition to be high-NO, a significantly long  
298  $\tau_{NO}$  is required. In OFR254-iNO,  $\tau_{NO}$  is so short that no good high-NO condition is found in the explored  
299 range in this study (Fig. 3a). A fraction of explored conditions are bad high-NO. These conditions result  
300 from a full consumption of  $O_3$  by NO. Then very little  $HO_x$  is produced, but the fate of any  $RO_2$  formed is  
301 dominated by  $RO_2+NO$ . However, also due to negligibly low OH concentration, little  $RO_2$  is produced and  
302 non-tropospheric photolysis of VOCs is also substantial compared to their reaction with OH under these  
303 conditions, classifying all of them as “bad.”

304 In OFR185-iNO, in addition to the typical case shown in Fig. 1a, many other cases have a  $\tau_{NO}$  of  
305  $\sim 10$  s or longer (Fig. S3), which allow the possibility of high-NO conditions. Indeed,  $\sim 1/3$  of explored  
306 conditions in OFR185-iNO with a residence time of 3 min are high-NO (Fig. 3b). Most of these high-NO  
307 conditions are also classified as bad, similar with those in OFR254-iNO. More importantly, in contrast to  
308 OFR254-iNO, good and risky high-NO conditions also comprise an appreciable fraction of the OFR185-  
309 iNO conditions. It is easily expected that very high  $OHR_{ext}$  and  $NO^{in}$  lead to bad high-NO conditions (Fig.  
310 4), since they strongly suppress  $HO_x$ , which yields bad conditions and in turn keep NO destruction  
311 relatively low. Besides, the occurrence of bad high-NO conditions is reduced at high UV, which can be  
312 explained by lowered NO due to high  $O_3$  production at high UV. Good high-NO conditions are rare in the  
313 explored space. They are only 1.1% of total explored conditions and present under very specific  
314 conditions, i.e., higher  $H_2O$ , lower UV, lower  $OHR_{ext}$ , and  $NO^{in}$  of tens to hundreds of ppb (Figs. 4 and  
315 S4). Since a very high NO can suppress OH, to obtain both a significant NO level and a good conditions,  
316  $NO^{in}$  can only be tens to hundreds of ppb. As  $NO^{in}$  is lower and OH is higher than under bad high-NO  
317 conditions, UV should be lower than bad high-NO conditions to keep a sufficiently long presence of NO.  
318 Thus, UV at 185 nm for good high-NO conditions are generally lower than  $10^{12}$  photons  $cm^{-2} s^{-1}$  (Fig. S4),  
319 which is also the UV criterion set for the good region in Peng et al. (2016). In addition, a low  $OHR_{ext}$   
320 (generally  $< 50 s^{-1}$ ) and a higher  $H_2O$  (the higher the better, although there is no apparent threshold) are  
321 also required for good high-NO conditions (Fig. S4), as Peng et al. (2016) pointed out. Risky high-NO  
322 conditions often occur between good and bad high-NO conditions, e.g., at lower  $NO^{in}$  than bad  
323 conditions (e.g., Cases ML, MM, HL, and HM), at higher  $OHR_{ext}$  and/or  $NO^{in}$  than good conditions (e.g.,  
324 Cases ML and MM), and at lower  $H_2O$  than good conditions (e.g., Case LL).

325 The trend of the distributions of good, risky, and bad low-NO conditions is generally in line with  
326 the analysis in Peng et al. (2016). For low-NO conditions,  $NO_y$  species can be simply regarded as external  
327 OH reactants, as Peng et al. (2016) did. As  $H_2O$  decreases and/or  $OHR_{ext}$  or  $NO^{in}$  increases, a low-NO  
328 condition becomes worse (good  $\rightarrow$  risky  $\rightarrow$  bad). In OFR185-iNO, increasing UV generally makes a low-NO  
329 condition better because of an OH production enhancement; while in OFR254-iNO, increasing UV  
330 generally makes a low-NO condition worse, since at a higher UV, more  $O_3$  is destroyed and the resilience  
331 of OH to suppression is reduced.

332 As discussed above, the fraction of high-NO conditions also depends on OFR residence time. A  
333 shorter residence time is expected to generally lead to a larger fraction of high-NO conditions, since the  
334 time spent in the reaction for  $t > \tau_{NO}$  is significantly smaller. Thus, we also investigate an OFR185-iNO



335 case with a residence time of 30 s. In Fig. 3b, compared to the case with a residence time of 3 min, the  
336 distributions of all condition types (good/risky/bad) of the 30 s residence time case shift toward higher  
337  $r(\text{RO}_2+\text{NO})/r(\text{RO}_2+\text{HO}_2)$ . Nevertheless, shortening the residence time also removes the period when the  
338 condition is better (i.e., less non-tropospheric photolysis), when external OH reactants have been  
339 partially consumed and OH suppression due to  $\text{OHR}_{\text{ext}}$  has been reduced later in the residence time. As  
340 a result, the fractions of good and risky conditions decrease. With the two effects (higher  
341  $r(\text{RO}_2+\text{NO})/r(\text{RO}_2+\text{HO}_2)$  and more significant non-tropospheric photolysis) combined, the fraction of  
342 good high-NO conditions increases by a factor of  $\sim 3$ . An even shorter residence time does not result in  
343 a larger good high-NO fraction, since the effect of enhancing non-tropospheric photolysis is even more  
344 apparent.

### 345 3.3 Possible issues related to high- $\text{NO}_x$ levels

346 In the discussion above, we focused on obtaining high-NO conditions and considered only one  
347 experimental issue (non-tropospheric photolysis) that had been previously investigated in Peng et al.  
348 (2016) and is not specific for experiments with high NO injection. We discuss additional potential  
349 reasons why the OFR-iNO chemistry can deviate strongly from tropospheric conditions, as specifically  
350 related to high- $\text{NO}_x$  level in this subsection.

#### 351 3.3.1 $\text{NO}_2$

352  $\text{NO}_2$  reacts with  $\text{RO}_2$  to form peroxy nitrates, generally regarded as reservoir species in the  
353 atmosphere as most of them thermally decompose very quickly compared to atmospheric time scales.  
354 However, in OFRs, with residence times on the order of minutes, some peroxy nitrates may no longer be  
355 considered as fast decomposing. This is especially true for acylperoxy nitrates, whose lifetimes can be  
356 hours at room temperature (Orlando and Tyndall, 2012). Acylperoxy nitrates are essentially sinks instead  
357 of reservoirs in OFRs for both  $\text{NO}_2$  and  $\text{RO}_2$ .  $\text{RO}_2$  is estimated to be as high as several ppb in OFRs by our  
358 model (e.g.,  $\sim 6$  ppb  $\text{RO}_2$  in OFR185 at  $\text{H}_2\text{O}=1\%$ , UV at  $185\text{ nm}=1\times 10^{13}$  photons  $\text{cm}^{-2}\text{ s}^{-1}$ ,  $\text{OHR}_{\text{ext}}=1000\text{ s}^{-1}$ ,  
359 and  $\text{NO}^{\text{in}}=0$ ), while high-NO experiments can yield far higher  $\text{NO}_2$ . If all  $\text{RO}_2$  were acylperoxy, the  $\text{RO}_2$   
360 chemistry could be rapidly shut down by  $\text{NO}_2$ , as rate constants of these  $\text{RO}_2 + \text{NO}_2$  reactions are around  
361  $10^{-11}\text{ cm}^3\text{ molecule}^{-1}\text{ s}^{-1}$  (Orlando and Tyndall, 2012). Nevertheless, acylperoxy nitrates are not expected  
362 to typically be the dominant component of peroxy nitrates, since acyl radicals are not a direct oxidation  
363 product of most common VOCs and can only be formed after several steps of oxidation (Atkinson and  
364 Arey, 2003; Ziemann and Atkinson, 2012). Most alkylperoxy nitrates retain their short-lived reservoir  
365 characteristics in OFRs due to their relatively short thermal decomposition time scales (on the order of  
366 0.1 s; Orlando and Tyndall, 2012). Even so, OFR experiments can be seriously hampered at extremely  
367 high  $\text{NO}_2$ . If  $\text{NO}_2$  reaches ppm levels, the equilibrium between  $\text{RO}_2+\text{NO}_2$  and alkylperoxy nitrate  
368 ( $\text{RO}_2+\text{NO}_2\leftrightarrow\text{RO}_2\text{NO}_2$ ) is greatly shifted toward the alkylperoxy nitrate side, as the forward and reverse  
369 rate constants are on the order of  $10^{-12}\text{ cm}^3\text{ molecule}^{-1}\text{ s}^{-1}$  and  $1\text{ s}^{-1}$ , respectively (Orlando and Tyndall,  
370 2012). This results in a substantial decrease in effective  $\text{RO}_2$  concentration, or in other words, a  
371 substantial slow-down of  $\text{RO}_2$  chemistry.

372 Parts per million levels of  $\text{NO}_2$  may impose an additional experimental artifact in the oxidation



373 chemistry of aromatic precursors. OH-aromatic adducts, i.e., the immediate products of aromatic  
374 oxidation by OH, undergo addition of O<sub>2</sub> and NO<sub>2</sub> at comparable rates under ppm levels of NO<sub>2</sub> (rate  
375 constants of the additions of O<sub>2</sub> and NO<sub>2</sub> are on the order of 10<sup>-16</sup> and 10<sup>-11</sup> molecules cm<sup>-3</sup> s<sup>-1</sup>,  
376 respectively ;Atkinson and Arey, 2003). However, only the former addition is atmospherically relevant  
377 (Calvert et al., 2002). Liu et al. (2015) performed OFR254-iNO experiments with toluene over a range of  
378 NO<sup>in</sup> of 2.5–10 ppm, encompassing the NO concentration range at which the reactions of OH-toluene  
379 adduct with O<sub>2</sub> and with NO<sub>2</sub> are of equal importance (~5 ppm; Atkinson and Arey, 2003). This suggests  
380 that nitroaromatics, whose formation was reported in the study of Liu et al. (2015), might have been  
381 formed in substantial amounts in that study through the addition of NO<sub>2</sub> to the OH-toluene adduct.

### 382 3.3.2 NO<sub>3</sub>

383 As discussed in Section 3.1, NO<sub>3</sub> can be formed in significant amounts in OFRs with high NO  
384 injection. Although NO<sub>3</sub> is also present in the atmosphere, especially during nighttime, significant VOC  
385 oxidation by both OH and NO<sub>3</sub> results in more complex chemistry that may complicate the  
386 interpretation of experimental results. NO<sub>3</sub> oxidation-only OFR has been previously realized  
387 experimentally via thermal dissociation of injected N<sub>2</sub>O<sub>5</sub> (Palm et al., 2017). We discuss below how to  
388 avoid significant VOC oxidation by NO<sub>3</sub> and achieve OH-dominated VOC oxidation in OFRs with high NO  
389 injection.

390 If NO<sub>3exp</sub>/OH<sub>exp</sub> > 0.1, NO<sub>3</sub> can be a competitive reactant for biogenic alkenes and dihydrofurans,  
391 which have a C=C bond for NO<sub>3</sub> addition, and phenols, which have activated hydroxyl for fast hydrogen  
392 abstraction by NO<sub>3</sub> (Atkinson and Arey, 2003), while for lower NO<sub>3exp</sub>/OH<sub>exp</sub>, OH is expected to dominate  
393 the oxidation of all VOCs, as shown in Fig. 6. Oxidation for VOCs without alkene C=C bonds and phenol  
394 hydroxyl (such as alkanes and (alkyl)benzenes) is dominated by OH unless NO<sub>3exp</sub>/OH<sub>exp</sub> > 1000. Despite  
395 its double bond, ethene reacts as slowly with NO<sub>3</sub> as alkanes, likely due to lack of alkyl groups enriching  
396 electron density on the C=C bond, which slows NO<sub>3</sub> addition. We calculate NO<sub>3exp</sub>/OH<sub>exp</sub> for OFR185-  
397 iNO and OFR254-iNO and plot histograms of this ratio in Fig. 6. Many experimental conditions lead to  
398 high enough NO<sub>3exp</sub>/OH<sub>exp</sub> that NO<sub>3</sub> is a competitive sink for alkenes, while only under very extreme  
399 conditions can NO<sub>3</sub> be a competitive sink for species without C=C bonds. High-NO conditions in OFR185-  
400 iNO have lower NO<sub>3exp</sub>/OH<sub>exp</sub> (~10<sup>-2</sup>–10<sup>2</sup>) than in OFR254-iNO (~10<sup>1</sup>–10<sup>5</sup>). This difference in NO<sub>3exp</sub>/OH<sub>exp</sub>  
401 is due to the different levels of O<sub>3</sub> in the two modes, as high O<sub>3</sub> promotes NO<sub>2</sub>-to-NO<sub>3</sub> oxidation. Note  
402 that low-NO conditions in both OFR185-iNO and OFR254-iNO can also reach high NO<sub>3exp</sub>/OH<sub>exp</sub> as some  
403 high-NO conditions have. This is because in OFR185-iNO a large part of NO<sub>3</sub> is formed by OH oxidation,  
404 resulting in NO<sub>3exp</sub>/OH<sub>exp</sub> being largely influenced by NO<sup>in</sup> but not by other factors mainly governing OH;  
405 and under low-NO conditions in OFR254-iNO, NO<sub>3</sub> can form rapidly from NO<sub>2</sub>+O<sub>3</sub>, while OH can be  
406 heavily suppressed by high OHR<sub>ext</sub>.

407 Most of the species shown in Fig. 6 are primary VOCs, except phenols and a dihydrofuran, which  
408 can be intermediates of the atmospheric oxidation of (alkyl)benzenes (Atkinson and Arey, 2003) and  
409 long-chain alkanes (Aimanant and Ziemann, 2013; Strollo and Ziemann, 2013; Ranney and Ziemann,  
410 2016), respectively. Nevertheless, only the phenol production may occur in high-NO OFRs, as the



411 particle-phase reaction in the photochemical formation of dihydrofurans from alkanes is too slow  
412 compared to typical OFR residence times (Ranney and Ziemann, 2016). Therefore, the impact of NO<sub>3</sub>  
413 oxidation on VOC fate needs to be considered only if the OFR input flow contains high NO mixed with  
414 biogenics and/or aromatics [(alkyl)benzenes and/or phenols]. However, (alkyl)benzenes were likely to  
415 be major SOA precursors in, to our knowledge, the only few literature OFR studies with high NO levels  
416 (Ortega et al., 2013; Tkacik et al., 2014; Liu et al., 2015). In the study of the air in a traffic tunnel (OFR185-  
417 iNO mode; Tkacik et al., 2014), where toluene is usually a major anthropogenic SOA precursor as in  
418 other urban environments (Dzepina et al., 2009; Borbon et al., 2013; Hayes et al., 2015; Jathar et al.,  
419 2015), NO<sub>x</sub> was several hundreds of ppb. This resulted in an estimated NO<sub>3exp</sub>/OH<sub>exp</sub> range of ~0.1–1,  
420 where up to ~30% of cresols (intermediates of toluene oxidation) may have been consumed by NO<sub>3</sub>.  
421 Dihydrofurans may also have formed in the tunnel air (but outside the OFR) in the presence of NO<sub>x</sub>  
422 (Aimanant and Ziemann, 2013; Strollo and Ziemann, 2013) and, after entering the OFR, they would have  
423 been substantially (up to ~50%) consumed by NO<sub>3</sub>. In the laboratory experiment of Liu et al. (2015) with  
424 toluene, the injection of as much as 10 ppm NO elevated NO<sub>3exp</sub>/OH<sub>exp</sub> to ~100, where cresols from  
425 toluene oxidation reacted almost exclusively with NO<sub>3</sub> in addition to being photolyzed.

### 426 3.3.3 A case study

427 We use a case study of an OFR254-13-iNO laboratory experiment with a large amount of toluene  
428 (5 ppm) and NO<sup>in</sup> (10 ppm) to illustrate how very high VOC and NO concentrations cause multiple types  
429 of atmospherically irrelevant reactions in OFR. Due to very high OHR<sub>ext</sub> and NO<sup>in</sup>, photolysis of toluene  
430 at 254 nm may have been important (Peng et al., 2016). In case of a high (close to 1) quantum yield, up  
431 to ~80% of the consumed toluene in their experiments could have been photolyzed (Scheme 1). Of the  
432 rest of reacted toluene, ~10% undergoes H-abstraction by OH from the methyl group in the model,  
433 leading to an RO<sub>2</sub> similar to alkyl RO<sub>2</sub> and likely proceeding with normal RO<sub>2</sub> chemistry. ~90% of the  
434 toluene formed an OH-adduct (Calvert et al., 2002). As discussed above, 70% of this adduct (depending  
435 on NO<sup>in</sup>) is predicted to recombine with NO<sub>2</sub> producing nitroaromatics because of the ppm-level NO<sub>x</sub>.  
436 The adduct could also react with O<sub>2</sub> via two types of pathways, of which one was addition forming a  
437 special category of RO<sub>2</sub> (OH-toluene-O<sub>2</sub> adducts) potentially undergoing ring-opening (Atkinson and  
438 Arey, 2003; Orlando and Tyndall, 2012; Ziemann and Atkinson, 2012), the other H-elimination by O<sub>2</sub>  
439 producing cresols. Again, like toluene, cresols may have been substantially photolyzed. As a result of  
440 NO<sub>3exp</sub>/OH<sub>exp</sub> ~100, only a minor portion of cresols could have repeated OH-addition–H-elimination  
441 process forming methyl-dihydroxybenzenes and other OH-oxidation products (Atkinson and Arey, 2003).  
442 The rest of cresols may have formed methylphenoxy radicals, nevertheless, dominantly via H-  
443 abstraction by NO<sub>3</sub>, since H-abstraction by OH was even a minor pathway compared to the OH-addition  
444 one (Atkinson et al., 1992). In summary, the model results suggest that there were two possible routes  
445 leading to nitroaromatic formation. However, one of them was likely of little atmospheric relevance due  
446 to very high NO<sub>x</sub> and the other occurs in the atmosphere but is not a major fate of aromatics (Calvert et  
447 al., 2002).

### 448 3.4 Implications for OFR experiments with combustion emissions as input



449 Emissions from combustion sources, e.g., vehicles and biomass burning, usually contain VOCs  
450 and NO<sub>x</sub> at very high concentrations (Table 1). An injection of this type of emissions (typically with OHR<sub>ext</sub>  
451 of thousands of s<sup>-1</sup> or larger and NO<sup>in</sup> of tens of ppm or larger) in OFRs without any pretreatment is likely  
452 to cause all experimental issues discussed in Peng et al. (2016) and this paper, i.e., strong OH  
453 suppression, substantial non-tropospheric photolysis, strong RO<sub>2</sub> suppression by NO<sub>2</sub> whether RO<sub>2</sub> is  
454 acyl RO<sub>2</sub> or not, fast reactions of NO<sub>2</sub> with OH-aromatic hydrocarbon adducts, substantial NO<sub>3</sub>  
455 contribution to VOC fate, and even a near-total inhibition of OFR chemistry due to complete titration of  
456 O<sub>3</sub> by NO in the case of OFR254. We take the study of Karjalainen et al. (2016), who used an OFR to  
457 oxidize diluted car exhaust in real-time, as an case study to investigate the extent to which these issues  
458 may affect typical combustion source studies and to explore approaches to mitigate the problems.

459 During the first 200 s of their experiment (defined as the “cold start” period when the catalyst is  
460 cold and emissions are high), NO and total hydrocarbon in the emissions of the test vehicle reached  
461 ~400 and ~600 ppm, respectively. We first simulate the oxidation of those emissions without any  
462 dilution (even though x12 dilution was used in their experiments) to explore the most extreme  
463 conditions. Our model simulation indicates that such an extremely concentrated source would generally  
464 lead to bad high- or low-NO conditions (depending on NO concentration) in their OFR (Fig. 7), even  
465 though it was run at relatively high H<sub>2</sub>O and UV. OH suppression can as high as 3 orders of magnitude;  
466 VOC fates by non-tropospheric photolysis and reactions of alkenes and phenols with NO<sub>3</sub> can be nearly  
467 100%; up to ~1/3 of OH-toluene adduct may be recombined with NO<sub>2</sub> instead of forming an adduct with  
468 O<sub>2</sub>. After the test vehicle entered the “hot stabilized” stage (200–1000 s), its VOC emissions (on the  
469 order of ppm) were still too high for an undiluted OFR to yield a good condition (Fig. S5). OH suppression  
470 can still reach 2 orders of magnitude; non-tropospheric photolysis, and sometimes reactions with NO<sub>3</sub>,  
471 can still dominate over reactions with OH in VOC fates; reactions of OH-toluene adduct with NO<sub>2</sub> can  
472 still be substantial at some small NO emission spikes. Moreover, although NO emissions were roughly  
473 at ppm level even during the hot stabilized period, NO effective lifetime may be very short during that  
474 period, leading to low-NO conditions in their OFR.

475 As suggested in Peng et al. (2016) for low-NO OFR, dilution of sources can also mitigate strong  
476 deviations on OFR-iNO chemistry vs. atmospherically-relevant conditions. A dilution by a factor of 12,  
477 as actually used by Karjalainen et al. (2016), appears to be sufficient to bring most hot stabilized period  
478 under good conditions (Fig. S5). However, most VOC, or in other words, most SOA formation potential,  
479 was emitted during the cold start period, when risky and bad conditions still prevailed (Figs. 7 and 8).  
480 Even if the emissions are diluted by x100, the cold-start emission peak (Fig. 7) is still under risky  
481 conditions. Although bad conditions are eliminated and good condition is present during most of time,  
482 this emission peak under risky condition may contribute >50% to total SOA formation potential (Fig. 8).  
483 For SOA formed under good condition to be dominant, a dilution factor >400 would be needed.

484 Note that the emissions of the test vehicle of Karjalainen et al. (2016) are rather clean compared  
485 to the typical 2013 US on-road fleet (i.e., all at the hot stabilized stage) measured by Bishop and  
486 Stedman (2013) (Figs. 9 and S6). For emissions of an average on-road fleet, a dilution by a factor of 100



487 or larger would be necessary to ensure that most emissions would be processed in OFR185 under good  
488 conditions at the highest H<sub>2</sub>O and UV in this study (Figs. 9b and S6b,e,h). In the case of lower H<sub>2</sub>O and/or  
489 UV, an even larger dilution factor would be required.

490 Conducting OFR185-iNO experiments at high UV lowers the dilution factor needed for good  
491 conditions. However, it also renders good high-NO condition impossible (see Section 3.2 and Fig. S4). If  
492 one wants to oxidize vehicle exhausts in a high-NO environment in OFR, as in an urban atmosphere,  
493 OFR185 at low UV is necessary. Consequently, a much stronger dilution is in turn necessary to keep the  
494 operation condition still good. Nevertheless, not all vehicle emissions can be moved into good high-NO  
495 region through a simple dilution (Figs. 9c and S6c,f,i). Furthermore, a low UV would seriously limit the  
496 highest OH<sub>exp</sub> that OFR can achieve ( $\sim 3 \times 10^{11}$  molecules cm<sup>-3</sup> s for modeled good high-NO conditions in  
497 this study), while a much higher OH<sub>exp</sub> would be desirable to fully convert SOA formation potential into  
498 measurable SOA mass. If both good high-NO condition and high OH<sub>exp</sub> are required, new techniques  
499 (e.g., injection of N<sub>2</sub>O at percent level proposed by Lambe et al. (2017)) may be necessary.

#### 500 4 Conclusions

501 In this study, OFR chemistry involving NO<sub>y</sub> species was systematically investigated over a wide  
502 range of conditions. NO initially injected into the OFR was found to be rapidly oxidized under most  
503 conditions. In particular, due to high O<sub>3</sub> concentrations, NO lifetime in OFR254-iNO was too short to  
504 result in a significant RO<sub>2</sub> consumption by NO compared to that by HO<sub>2</sub> under all conditions with active  
505 chemistry. Nevertheless, it is not completely impossible for OFR185-iNO to have a significant RO<sub>2</sub> fate  
506 by NO and minor non-tropospheric photolysis at the same time (“good high-NO conditions”). According  
507 to our simulations, these conditions are most likely present at high H<sub>2</sub>O, low UV, low OHR<sub>ext</sub>, and NO<sup>in</sup>  
508 of tens to hundreds of ppb.

509 However, many past OFR studies with high NO injection were conducted under conditions  
510 remarkably different from the abovementioned very narrow range. NO<sup>in</sup> and/or OHR<sub>ext</sub> in those studies  
511 were often much higher than good high-NO conditions require (particularly, >3 orders of magnitude in  
512 some OFR studies using combustion emissions as input). In addition to non-tropospheric organic  
513 photolysis, OFR oxidation of highly concentrated sources can cause multiple large deviations from  
514 tropospheric OH oxidation, i.e., RO<sub>2</sub> suppression by high NO<sub>2</sub>, substantial nitroaromatic formation from  
515 the recombination of NO<sub>2</sub> and OH-aromatic adducts, and fast reactions of VOCs with NO<sub>3</sub> compared to  
516 those with OH.

517 Working at lower NO<sub>x</sub> (sub-ppm level) and VOC concentrations or dilution can mitigate these  
518 experimental problems. In general, a strong dilution (by a factor of >100) is needed for OFR that process  
519 typical on-road vehicle emissions. Humidification can also make good conditions more likely. By these  
520 measures, good conditions can be guaranteed, as long as NO and/or precursor concentrations are  
521 sufficiently low, while high-NO conditions cannot be ensured. To aid design and interpretation of OFR  
522 experiments with high NO injection, we provide our detailed modeling results in a visualized form (Fig.  
523 S7). For OFR users in need for both high OH<sub>exp</sub> and high NO, simple NO injection is not a good option.  
524 New techniques (e.g., injection of N<sub>2</sub>O proposed by Lambe et al. (2017) or other innovations) may be



525 necessary to meet this need.

526

527

528 **Acknowledgements**

529 This work was partially supported by DOE (BER/ASR) DE-SC0011105 & DE-SC0016559, EPA STAR  
530 83587701-0, and NSF AGS-1360834. We thank Pengfei Liu, Andrew Lambe, and Daniel Tkacik for  
531 providing some OFR experimental data, the authors of Karjalainen et al. (2016) and their project IEA-  
532 AMF Annex 44 for providing the data and information for the vehicle tests, Gary Bishop for providing  
533 on-road vehicle emission data, and Andrew Lambe and William Brune for useful discussions.  
534

535 **References**

- 536 Aimanant, S. and Ziemann, P. J.: Chemical Mechanisms of Aging of Aerosol Formed from the Reaction  
537 of n-Pentadecane with OH Radicals in the Presence of NO<sub>x</sub>, *Aerosol Sci. Technol.*, 47(9), 979–990,  
538 doi:10.1080/02786826.2013.804621, 2013.
- 539 Alanen, J., Simonen, P., Saarikoski, S., Timonen, H., Kangasniemi, O., Saukko, E., Hillamo, R., Lehtoranta,  
540 K., Murtonen, T., Vesala, H., Keskinen, J. and Rönkkö, T.: Comparison of primary and secondary particle  
541 formation from natural gas engine exhaust and of their volatility characteristics, *Atmos. Chem. Phys.*  
542 *Discuss.*, (February), 1–27, doi:10.5194/acp-2017-44, 2017.
- 543 Ammann, M., Cox, R. A., Crowley, J. N., Jenkin, M. E., Mellouki, A., Rossi, M. J., Troe, J., Wallington, T. J.,  
544 Cox, B., Atkinson, R., Baulch, D. L. and Kerr, J. A.: IUPAC Task Group on Atmospheric Chemical Kinetic  
545 Data Evaluation, [online] Available from: <http://iupac.pole-ether.fr/#>, 2016.
- 546 Atkinson, R. and Arey, J.: Atmospheric degradation of volatile organic compounds., *Chem. Rev.*, 103(12),  
547 4605–38, doi:10.1021/cr0206420, 2003.
- 548 Atkinson, R., Aschmann, S. M. and Arey, J.: Reactions of hydroxyl and nitrogen trioxide radicals with  
549 phenol, cresols, and 2-nitrophenol at 296 ± 2 K, *Environ. Sci. Technol.*, 26(7), 1397–1403,  
550 doi:10.1021/es00031a018, 1992.
- 551 BIPM, IEC, IFCC, ILAC, ISO, IUPAC and IUPAPOIML: JCGM 101: 2008 Evaluation of measurement data —  
552 Supplement 1 to the “ Guide to the expression of uncertainty in measurement ” — Propagation of  
553 distributions using a Monte Carlo method., 2008.
- 554 Bishop, G. A. and Stedman, D. H.: Fuel Efficiency Automobile Test: Light-Duty Vehicles, [online] Available  
555 from: [http://www.feat.biochem.du.edu/light\\_duty\\_vehicles.html](http://www.feat.biochem.du.edu/light_duty_vehicles.html) (Accessed 1 February 2017), 2013.
- 556 Borbon, A., Gilman, J. B., Kuster, W. C., Grand, N., Chevaillier, S., Colomb, A., Dolgorouky, C., Gros, V.,  
557 Lopez, M., Sarda-Esteve, R., Holloway, J., Stutz, J., Petetin, H., McKeen, S., Beekmann, M., Warneke, C.,  
558 Parrish, D. D. and De Gouw, J. A.: Emission ratios of anthropogenic volatile organic compounds in  
559 northern mid-latitude megacities: Observations versus emission inventories in Los Angeles and Paris, *J.*  
560 *Geophys. Res. Atmos.*, 118(4), 2041–2057, doi:10.1002/jgrd.50059, 2013.
- 561 Burkholder, J. B., Sander, S. P., Abbatt, J., Barker, J. R., Huie, R. E., Kolb, C. E., Kurylo, M. J., Orkin, V. L.,  
562 Wilmoth, D. M. and Wine, P. H.: Chemical Kinetics and Photochemical Data for Use in Atmospheric  
563 Studies: Evaluation Number 18, Pasadena, CA, USA. [online] Available from:  
564 <http://jpldataeval.jpl.nasa.gov/>, 2015.
- 565 Calvert, J. G., Atkinson, R., Becker, K. H., Kamens, R. M., Seinfeld, J. H., Wallington, T. H. and Yarwood,  
566 G.: The Mechanisms of Atmospheric Oxidation of the Aromatic Hydrocarbons, Oxford University Press,  
567 USA. [online] Available from: <https://books.google.com/books?id=P0basaLrxDMC>, 2002.
- 568 Carlton, A. G., Wiedinmyer, C. and Kroll, J. H.: A review of Secondary Organic Aerosol (SOA) formation  
569 from isoprene, *Atmos. Chem. Phys.*, 9(14), 4987–5005, doi:10.5194/acp-9-4987-2009, 2009.
- 570 Carter, W. P. L., Cocker, D. R., Fitz, D. R., Malkina, I. L., Bumiller, K., Sauer, C. G., Pisano, J. T., Bufalino, C.  
571 and Song, C.: A new environmental chamber for evaluation of gas-phase chemical mechanisms and  
572 secondary aerosol formation, *Atmos. Environ.*, 39(40), 7768–7788,  
573 doi:10.1016/j.atmosenv.2005.08.040, 2005.
- 574 Chameides, W., Lindsay, R., Richardson, J. and Kiang, C.: The role of biogenic hydrocarbons in urban  
575 photochemical smog: Atlanta as a case study, *Science* (80-. ), 241(4872), 1473–1475,  
576 doi:10.1126/science.3420404, 1988.
- 577 Cocker, D. R., Flagan, R. C. and Seinfeld, J. H.: State-of-the-Art Chamber Facility for Studying Atmospheric  
578 Aerosol Chemistry, *Environ. Sci. Technol.*, 35(12), 2594–2601, doi:10.1021/es0019169, 2001.
- 579 Dzepina, K., Volkamer, R. M., Madronich, S., Tulet, P., Ulbrich, I. M., Zhang, Q., Cappa, C. D., Ziemann, P.  
580 J. and Jimenez, J. L.: Evaluation of recently-proposed secondary organic aerosol models for a case study  
581 in Mexico City, *Atmos. Chem. Phys.*, 9(15), 5681–5709, doi:10.5194/acp-9-5681-2009, 2009.
- 582 George, I. J., Vlasenko, A., Slowik, J. G., Broekhuizen, K. and Abbatt, J. P. D.: Heterogeneous oxidation of  
583 saturated organic aerosols by hydroxyl radicals: uptake kinetics, condensed-phase products, and particle  
584 size change, *Atmos. Chem. Phys.*, 7(16), 4187–4201, doi:10.5194/acp-7-4187-2007, 2007.





- 585 Haagen-Smit, A. J.: Chemistry and Physiology of Los Angeles Smog, *Ind. Eng. Chem.*, 44(6), 1342–1346,  
586 doi:10.1021/ie50510a045, 1952.
- 587 Hallquist, M., Wenger, J. C., Baltensperger, U., Rudich, Y., Simpson, D., Claeys, M., Dommen, J., Donahue,  
588 N. M., George, C., Goldstein, A. H., Hamilton, J. F., Herrmann, H., Hoffmann, T., Iinuma, Y., Jang, M.,  
589 Jenkin, M. E., Jimenez, J. L., Kiendler-Scharr, A., Maenhaut, W., McFiggans, G., Mentel, T. F., Monod, A.,  
590 Prevot, A. S. H., Seinfeld, J. H., Surratt, J. D., Szmigielski, R. and Wildt, J.: The formation, properties and  
591 impact of secondary organic aerosol: current and emerging issues, *Atmos. Chem. Phys.*, 9(14), 5155–  
592 5236, 2009.
- 593 Hayes, P. L., Carlton, a. G., Baker, K. R., Ahmadov, R., Washenfelder, R. a., Alvarez, S., Rappenglück, B.,  
594 Gilman, J. B., Kuster, W. C., de Gouw, J. a., Zotter, P., Prévôt, a. S. H., Szidat, S., Kleindienst, T. E., Offenberg,  
595 J. H., Ma, P. K. and Jimenez, J. L.: Modeling the formation and aging of secondary organic aerosols in Los  
596 Angeles during CalNex 2010, *Atmos. Chem. Phys.*, 15(10), 5773–5801, doi:10.5194/acp-15-5773-2015,  
597 2015.
- 598 Hoffmann, T., Odum, J. R., Bowman, F., Collins, D., Klockow, D., Flagan, R. C. and Seinfeld, J. H.:  
599 Formation of Organic Aerosols from the Oxidation of Biogenic Hydrocarbons, *J. Atmos. Chem.*, 26(2),  
600 189–222, doi:10.1023/A:1005734301837, 1997.
- 601 Jathar, S. H., Cappa, C. D., Wexler, a. S., Seinfeld, J. H. and Kleeman, M. J.: Multi-generational oxidation  
602 model to simulate secondary organic aerosol in a 3-D air quality model, *Geosci. Model Dev.*, 8(8), 2553–  
603 2567, doi:10.5194/gmd-8-2553-2015, 2015.
- 604 Kang, E., Root, M. J., Toohey, D. W. and Brune, W. H.: Introducing the concept of Potential Aerosol Mass  
605 (PAM), *Atmos. Chem. Phys.*, 7(22), 5727–5744, doi:10.5194/acp-7-5727-2007, 2007.
- 606 Kang, E., Toohey, D. W. and Brune, W. H.: Dependence of SOA oxidation on organic aerosol mass  
607 concentration and OH exposure: experimental PAM chamber studies, *Atmos. Chem. Phys.*, 11(4), 1837–  
608 1852, doi:10.5194/acp-11-1837-2011, 2011.
- 609 Karjalainen, P., Timonen, H., Saukko, E., Kuuluvainen, H., Saarikoski, S., Aakko-Saksa, P., Murtonen, T.,  
610 Bloss, M., Dal Maso, M., Simonen, P., Ahlberg, E., Svenningsson, B., Brune, W. H., Hillamo, R., Keskinen,  
611 J. and Rönkkö, T.: Time-resolved characterization of primary particle emissions and secondary particle  
612 formation from a modern gasoline passenger car, *Atmos. Chem. Phys.*, 16(13), 8559–8570,  
613 doi:10.5194/acp-16-8559-2016, 2016.
- 614 Krechmer, J. E., Pagonis, D., Ziemann, P. J. and Jimenez, J. L.: Quantification of Gas-Wall Partitioning in  
615 Teflon Environmental Chambers Using Rapid Bursts of Low-Volatility Oxidized Species Generated in Situ,  
616 *Environ. Sci. Technol.*, 50(11), 5757–5765, doi:10.1021/acs.est.6b00606, 2016.
- 617 Lambe, A., Massoli, P., Zhang, X., Canagaratna, M., Nowak, J., Yan, C., Nie, W., Onasch, T., Jayne, J., Kolb,  
618 C., Davidovits, P., Worsnop, D. and Brune, W.: Controlled nitric oxide production via  
619  $O(\text{sup&gt;1&gt;})+N(\text{sub&gt;2&gt;})O$  reactions for use in oxidation flow reactor studies, *Atmos. Meas. Tech. Discuss.*, (January), 1–20,  
620 doi:10.5194/amt-2016-394, 2017.
- 622 Lambe, A. T., Ahern, A. T., Williams, L. R., Slowik, J. G., Wong, J. P. S., Abbatt, J. P. D., Brune, W. H., Ng, N.  
623 L., Wright, J. P., Croasdale, D. R., Worsnop, D. R., Davidovits, P. and Onasch, T. B.: Characterization of  
624 aerosol photooxidation flow reactors: heterogeneous oxidation, secondary organic aerosol formation  
625 and cloud condensation nuclei activity measurements, *Atmos. Meas. Tech.*, 4(3), 445–461,  
626 doi:10.5194/amt-4-445-2011, 2011.
- 627 Lambe, A. T. and Jimenez, J. L.: PAM Wiki: Publications Using the PAM Oxidation Flow Reactor, [online]  
628 Available from: <https://sites.google.com/site/pamwiki/publications> (Accessed 10 February 2017), 2017.
- 629 Levy II, H.: Normal atmosphere: large radical and formaldehyde concentrations predicted., *Science*,  
630 173(3992), 141–143, doi:10.1126/science.173.3992.141, 1971.
- 631 Li, R., Palm, B. B., Borbon, A., Graus, M., Warneke, C., Ortega, a M., Day, D. a, Brune, W. H., Jimenez, J.  
632 L. and de Gouw, J. a: Laboratory Studies on Secondary Organic Aerosol Formation from Crude Oil Vapors,  
633 *Environ. Sci. Technol.*, 47(21), 12566–12574, doi:10.1021/es402265y, 2013.
- 634 Li, R., Palm, B. B., Ortega, A. M., Hu, W., Peng, Z., Day, D. A., Knote, C., Brune, W. H., de Gouw, J. and  
635 Jimenez, J. L.: Modeling the radical chemistry in an Oxidation Flow Reactor (OFR): radical formation and



- 636 recycling, sensitivities, and OH exposure estimation equation, *J. Phys. Chem. A*, 119(19), 4418–4432,  
637 doi:10.1021/jp509534k, 2015.
- 638 Link, M. F., Friedman, B., Fulgham, R., Brophy, P., Galang, A., Jathar, S. H., Veres, P., Roberts, J. M. and  
639 Farmer, D. K.: Photochemical processing of diesel fuel emissions as a large secondary source of isocyanic  
640 acid (HNCO), *Geophys. Res. Lett.*, 43(8), 4033–4041, doi:10.1002/2016GL068207, 2016.
- 641 Lippmann, M.: Health effects of tropospheric ozone, *Environ. Sci. Technol.*, 25(12), 1954–1962,  
642 doi:10.1021/es00024a001, 1991.
- 643 Liu, P. F., Abdelmalki, N., Hung, H.-M., Wang, Y., Brune, W. H. and Martin, S. T.: Ultraviolet and visible  
644 complex refractive indices of secondary organic material produced by photooxidation of the aromatic  
645 compounds toluene and m-Xylene, *Atmos. Chem. Phys.*, 15(3), 1435–1446, doi:10.5194/acp-15-1435-  
646 2015, 2015.
- 647 Mao, J., Ren, X., Brune, W. H., Olson, J. R., Crawford, J. H., Fried, a., Huey, L. G., Cohen, R. C., Heikes, B.,  
648 Singh, H. B., Blake, D. R., Sachse, G. W., Diskin, G. S., Hall, S. R. and Shetter, R. E.: Airborne measurement  
649 of OH reactivity during INTEX-B, *Atmos. Chem. Phys.*, 9(1), 163–173, doi:10.5194/acp-9-163-2009, 2009.
- 650 Martinsson, J., Eriksson, A. C., Nielsen, I. E., Malmborg, V. B., Ahlberg, E., Andersen, C., Lindgren, R.,  
651 Nyström, R., Nordin, E. Z., Brune, W. H., Svenningsson, B., Swietlicki, E., Boman, C. and Pagels, J. H.:  
652 Impacts of Combustion Conditions and Photochemical Processing on the Light Absorption of Biomass  
653 Combustion Aerosol, *Environ. Sci. Technol.*, 49(24), 14663–14671, doi:10.1021/acs.est.5b03205, 2015.
- 654 Matsunaga, A. and Ziemann, P. J.: Gas-Wall Partitioning of Organic Compounds in a Teflon Film Chamber  
655 and Potential Effects on Reaction Product and Aerosol Yield Measurements, *Aerosol Sci. Technol.*, 44(10),  
656 881–892, doi:10.1080/02786826.2010.501044, 2010.
- 657 Nel, A.: Air Pollution-Related Illness: Effects of Particles, *Science* (80-. ), 308(5723), 804–806,  
658 doi:10.1126/science.1108752, 2005.
- 659 Ng, N. L., Canagaratna, M. R., Zhang, Q., Jimenez, J. L., Tian, J., Ulbrich, I. M., Kroll, J. H., Docherty, K. S.,  
660 Chhabra, P. S., Bahreini, R., Murphy, S. M., Seinfeld, J. H., Hildebrandt, L., Donahue, N. M., DeCarlo, P. F.,  
661 Lanz, V. a., Prévôt, a. S. H., Dinar, E., Rudich, Y., Worsnop, D. R., Prevot, A. S. H., Dinar, E., Rudich, Y. and  
662 Worsnop, D. R.: Organic aerosol components observed in Northern Hemispheric datasets from Aerosol  
663 Mass Spectrometry, *Atmos. Chem. Phys.*, 10(10), 4625–4641, doi:10.5194/acp-10-4625-2010, 2010.
- 664 Odum, J. R., Hoffmann, T., Bowman, F., Collins, D., Flagan Richard, C. and Seinfeld John, H.: Gas particle  
665 partitioning and secondary organic aerosol yields, *Environ. Sci. Technol.*, 30(8), 2580–2585,  
666 doi:10.1021/es950943+, 1996.
- 667 Orlando, J. J. and Tyndall, G. S.: Laboratory studies of organic peroxy radical chemistry: an overview with  
668 emphasis on recent issues of atmospheric significance, *Chem. Soc. Rev.*, 41(19), 6294,  
669 doi:10.1039/c2cs35166h, 2012.
- 670 Ortega, A. M., Day, D. A., Cubison, M. J., Brune, W. H., Bon, D., de Gouw, J. A. and Jimenez, J. L.:  
671 Secondary organic aerosol formation and primary organic aerosol oxidation from biomass-burning  
672 smoke in a flow reactor during FLAME-3, *Atmos. Chem. Phys.*, 13(22), 11551–11571, doi:10.5194/acp-  
673 13-11551-2013, 2013.
- 674 Ortega, A. M., Hayes, P. L., Peng, Z., Palm, B. B., Hu, W., Day, D. A., Li, R., Cubison, M. J., Brune, W. H.,  
675 Graus, M., Warneke, C., Gilman, J. B., Kuster, W. C., de Gouw, J., Gutiérrez-Montes, C. and Jimenez, J. L.:  
676 Real-time measurements of secondary organic aerosol formation and aging from ambient air in an  
677 oxidation flow reactor in the Los Angeles area, *Atmos. Chem. Phys.*, 16(11), 7411–7433,  
678 doi:10.5194/acp-16-7411-2016, 2016.
- 679 Palm, B. B., Campuzano-Jost, P., Day, D. A., Ortega, A. M., Fry, J. L., Brown, S. S., Zarzana, K. J., Dube, W.,  
680 Wagner, N. L., Draper, D. C., Kaser, L., Jud, W., Karl, T., Hansel, A., Gutiérrez-Montes, C. and Jimenez, J.  
681 L.: Secondary organic aerosol formation from in situ OH,  
682 O<sub>3</sub> and NO<sub>3</sub>, and NO<sub>2</sub> oxidation of ambient forest air in an oxidation flow reactor, *Atmos. Chem. Phys. Discuss.*, 1–46,  
683 doi:10.5194/acp-2016-1080, 2017.
- 685 Palm, B. B., Campuzano-Jost, P., Ortega, A. M., Day, D. A., Kaser, L., Jud, W., Karl, T., Hansel, A., Hunter, J.  
686 F., Cross, E. S., Kroll, J. H., Peng, Z., Brune, W. H. and Jimenez, J. L.: In situ secondary organic aerosol



- 687 formation from ambient pine forest air using an oxidation flow reactor, *Atmos. Chem. Phys.*, 16(5),  
688 2943–2970, doi:10.5194/acp-16-2943-2016, 2016.
- 689 Peng, Z., Carrasco, N. and Pernot, P.: Modeling of synchrotron-based laboratory simulations of Titan's  
690 ionospheric photochemistry, *GeoResJ*, 1–2, 33–53, doi:10.1016/j.grj.2014.03.002, 2014.
- 691 Peng, Z., Day, D. A., Ortega, A. M., Palm, B. B., Hu, W., Stark, H., Li, R., Tsigaridis, K., Brune, W. H. and  
692 Jimenez, J. L.: Non-OH chemistry in oxidation flow reactors for the study of atmospheric chemistry  
693 systematically examined by modeling, *Atmos. Chem. Phys.*, 16(7), 4283–4305, doi:10.5194/acp-16-  
694 4283-2016, 2016.
- 695 Peng, Z., Day, D. A., Stark, H., Li, R., Lee-Taylor, J., Palm, B. B., Brune, W. H. and Jimenez, J. L.: HOx radical  
696 chemistry in oxidation flow reactors with low-pressure mercury lamps systematically examined by  
697 modeling, *Atmos. Meas. Tech.*, 8(11), 4863–4890, doi:10.5194/amt-8-4863-2015, 2015.
- 698 Ranney, A. P. and Ziemann, P. J.: Kinetics of Acid-Catalyzed Dehydration of Cyclic Hemiacetals in Organic  
699 Aerosol Particles in Equilibrium with Nitric Acid Vapor, *J. Phys. Chem. A*, 120(16), 2561–2568,  
700 doi:10.1021/acs.jpca.6b01402, 2016.
- 701 Saltelli, A., Ratto, M., Tarantola, S. and Campolongo, F.: Sensitivity Analysis for Chemical Models, *Chem.*  
702 *Rev.*, 105(7), 2811–2828, doi:10.1021/cr040659d, 2005.
- 703 Sander, S. P., Friedl, R. R., Barker, J. R., Golden, D. M., Kurylo, M. J., Wine, P. H., Abbatt, J. P. D., Burkholder,  
704 J. B., Kolb, C. E., Moortgat, G. K., Huie, R. E. and Orkin, V. L.: Chemical Kinetics and Photochemical Data  
705 for Use in Atmospheric Studies Evaluation Number 17, Pasadena, CA, USA. [online] Available from:  
706 [http://jpldataeval.jpl.nasa.gov/pdf/JPL\\_10-6\\_Final\\_15June2011.pdf](http://jpldataeval.jpl.nasa.gov/pdf/JPL_10-6_Final_15June2011.pdf), 2011.
- 707 Schill, G. P., Jathar, S. H., Kodros, J. K., Levin, E. J. T., Galang, A. M., Friedman, B., Link, M. F., Farmer, D.  
708 K., Pierce, J. R., Kreidenweis, S. M. and DeMott, P. J.: Ice-nucleating particle emissions from  
709 photochemically aged diesel and biodiesel exhaust, *Geophys. Res. Lett.*, 43(10), 5524–5531,  
710 doi:10.1002/2016GL069529, 2016.
- 711 Seakins, P. W.: A brief review of the use of environmental chambers for gas phase studies of kinetics,  
712 chemical mechanisms and characterisation of field instruments, *EPJ Web Conf.*, 9, 143–163,  
713 doi:10.1051/epjconf/201009012, 2010.
- 714 Simonen, P., Saukko, E., Karjalainen, P., Timonen, H., Bloss, M., Aakko-Saksa, P., Rönkkö, T., Keskinen, J.  
715 and Dal Maso, M.: A New Oxidation Flow Reactor for Measuring Secondary Aerosol Formation of Rapidly  
716 Changing Emission Sources, *Atmos. Meas. Tech. Discuss.*, (November), 1–27, doi:10.5194/amt-2016-  
717 300, 2016.
- 718 Stocker, T. F., Qin, D., Plattner, G.-K., Tignor, M., Allen, S. K., Boschung, J., Nauels, A., Xia, Y., Bex, V. and  
719 Midgley, P. M.: *Climate Change 2013 - The Physical Science Basis*, edited by Intergovernmental Panel on  
720 Climate Change, Cambridge University Press, Cambridge., 2014.
- 721 Strollo, C. M. and Ziemann, P. J.: Products and mechanism of secondary organic aerosol formation from  
722 the reaction of 3-methylfuran with OH radicals in the presence of NOx, *Atmos. Environ.*, 77, 534–543,  
723 doi:10.1016/j.atmosenv.2013.05.033, 2013.
- 724 Tkacik, D. S., Lambe, A. T., Jathar, S., Li, X., Presto, A. A., Zhao, Y., Blake, D., Meinardi, S., Jayne, J. T.,  
725 Croteau, P. L. and Robinson, A. L.: Secondary Organic Aerosol Formation from in-Use Motor Vehicle  
726 Emissions Using a Potential Aerosol Mass Reactor, *Environ. Sci. Technol.*, 48(19), 11235–11242,  
727 doi:10.1021/es502239v, 2014.
- 728 Volkamer, R., Jimenez, J. L., San Martini, F., Dzepina, K., Zhang, Q., Salcedo, D., Molina, L. T., Worsnop,  
729 D. R. and Molina, M. J.: Secondary organic aerosol formation from anthropogenic air pollution: Rapid  
730 and higher than expected, *Geophys. Res. Lett.*, 33(17), L17811, doi:10.1029/2006GL026899, 2006.
- 731 Wang, J., Doussin, J. F., Perrier, S., Perraudin, E., Katrib, Y., Pangu, E. and Picquet-Varrault, B.: Design of  
732 a new multi-phase experimental simulation chamber for atmospheric photochemistry, aerosol and cloud  
733 chemistry research, *Atmos. Meas. Tech.*, 4(11), 2465–2494, doi:10.5194/amt-4-2465-2011, 2011.
- 734 Zhang, X., Cappa, C. D., Jathar, S. H., McVay, R. C., Ensberg, J. J., Kleeman, M. J. and Seinfeld, J. H.:  
735 Influence of vapor wall loss in laboratory chambers on yields of secondary organic aerosol., *Proc. Natl.*  
736 *Acad. Sci. U. S. A.*, 111(16), 5802–7, doi:10.1073/pnas.1404727111, 2014.

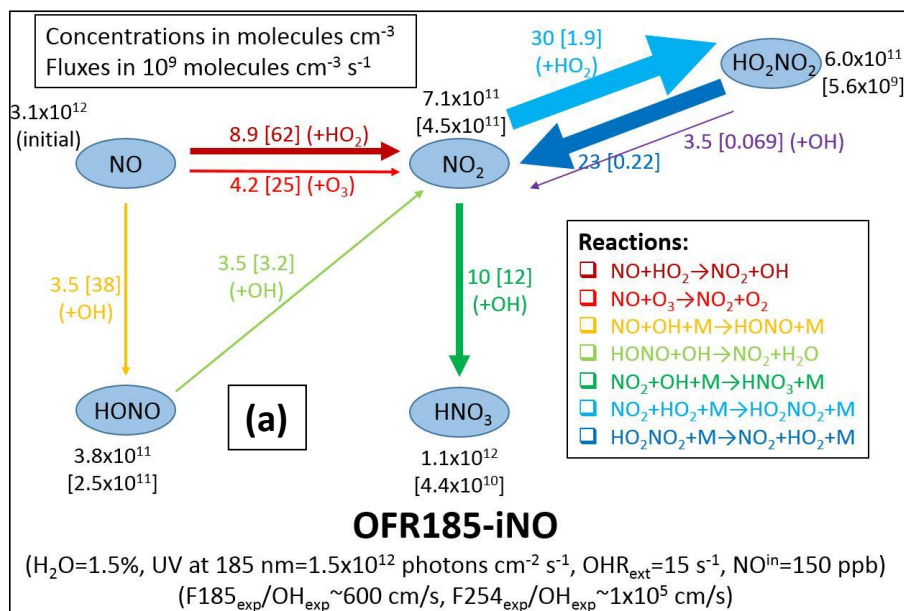


737 Ziemann, P. and Atkinson, R.: Kinetics, products, and mechanisms of secondary organic aerosol  
738 formation, *Chem. Soc. Rev.*, 41(19), 6582, doi:10.1039/c2cs35122f, 2012.

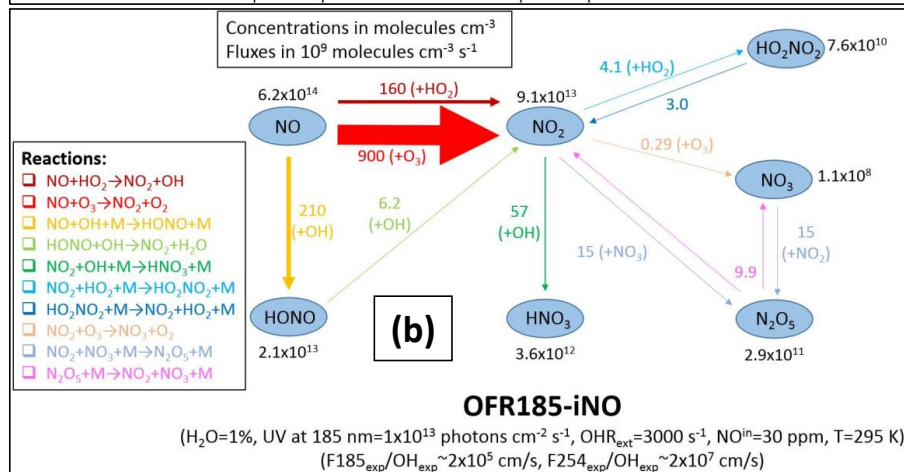
739

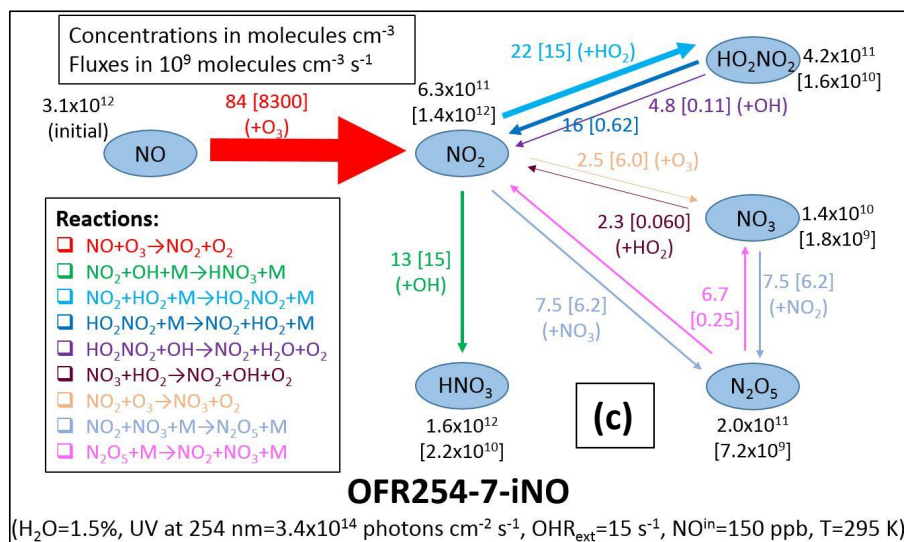


740

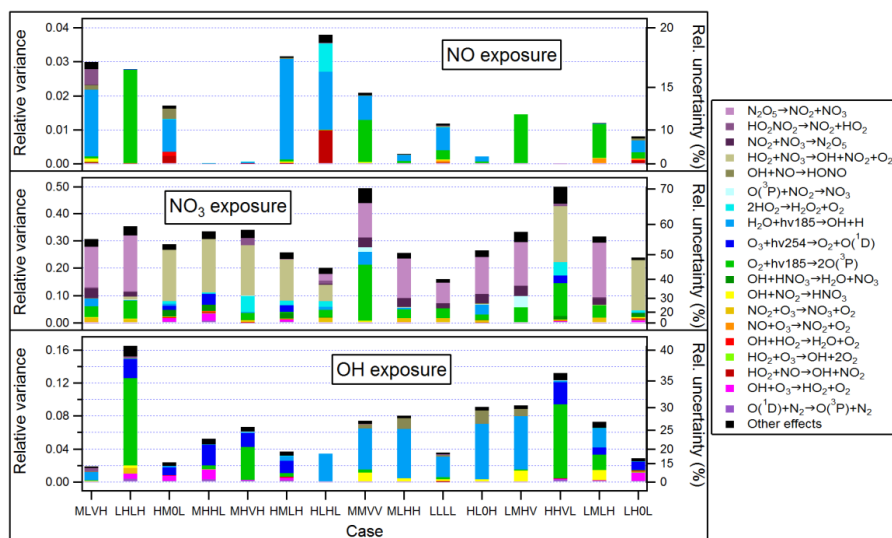


741



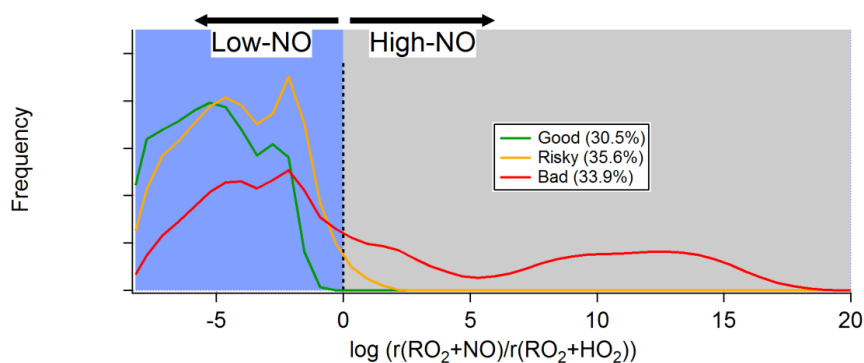


742  
 743 **Figure 1.** Schematics of main N-containing species and their major interconversion pathways under  
 744 typical input conditions for (a) OFR185-iNO with  $\text{NO}^{\text{in}}=150 \text{ ppb}$ , (b) OFR254-7-iNO with  $\text{NO}^{\text{in}}=150 \text{ ppb}$ ,  
 745 and (c) OFR185-iNO with  $\text{NO}^{\text{in}}=30 \text{ ppm}$ . Species average concentrations (in molecules  $\text{cm}^{-3}$ ) are shown  
 746 in black beside species names. Arrows denote directions of the conversions. Average reaction fluxes (in  
 747 units of  $10^9 \text{ molecules cm}^{-3} \text{ s}^{-1}$ ) are calculated according to the production rate, and shown on or beside  
 748 the corresponding arrows and in the same color. Within each schematic, the thickness of the arrows is  
 749 a measure of their corresponding species flux. Multiple arrows in the same color and pointing to the  
 750 same species should be counted only once for reaction flux on a species. Note that all values in these  
 751 schematics are average ones over the residence time, except for those in square brackets in panels a  
 752 and b, which are average values within approximate NO effective lifetime ( $\tau_{\text{NO}}$ , or more accurately, an  
 753 integer multiple of the model's output time step closest to NO effective lifetime). All concentrations and  
 754 fluxes have two significant digits.



755

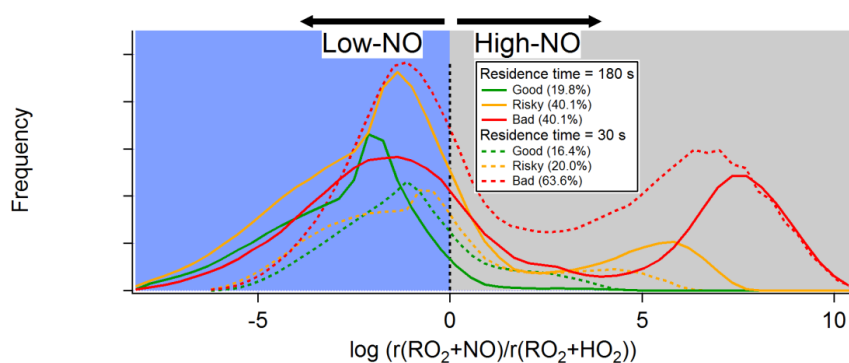
756 **Figure 2.** Relative variances (left axes)/uncertainties (right axes) of several outputs (i.e., NO, NO<sub>3</sub>, and  
 757 OH exposures) of Monte Carlo uncertainty propagation, and relative contributions of key reactions to  
 758 these relative variances in several typical cases in OFR185-iNO. Relative variances are shown in linear  
 759 scales (left axis), while corresponding relative uncertainties, equal to relative variances' square roots,  
 760 are indicated by the non-linear right axis. Only the reactions with a contribution of no less than 0.04 to  
 761 at least one relative variance are shown.



762

763

(a) OFR254-iNO



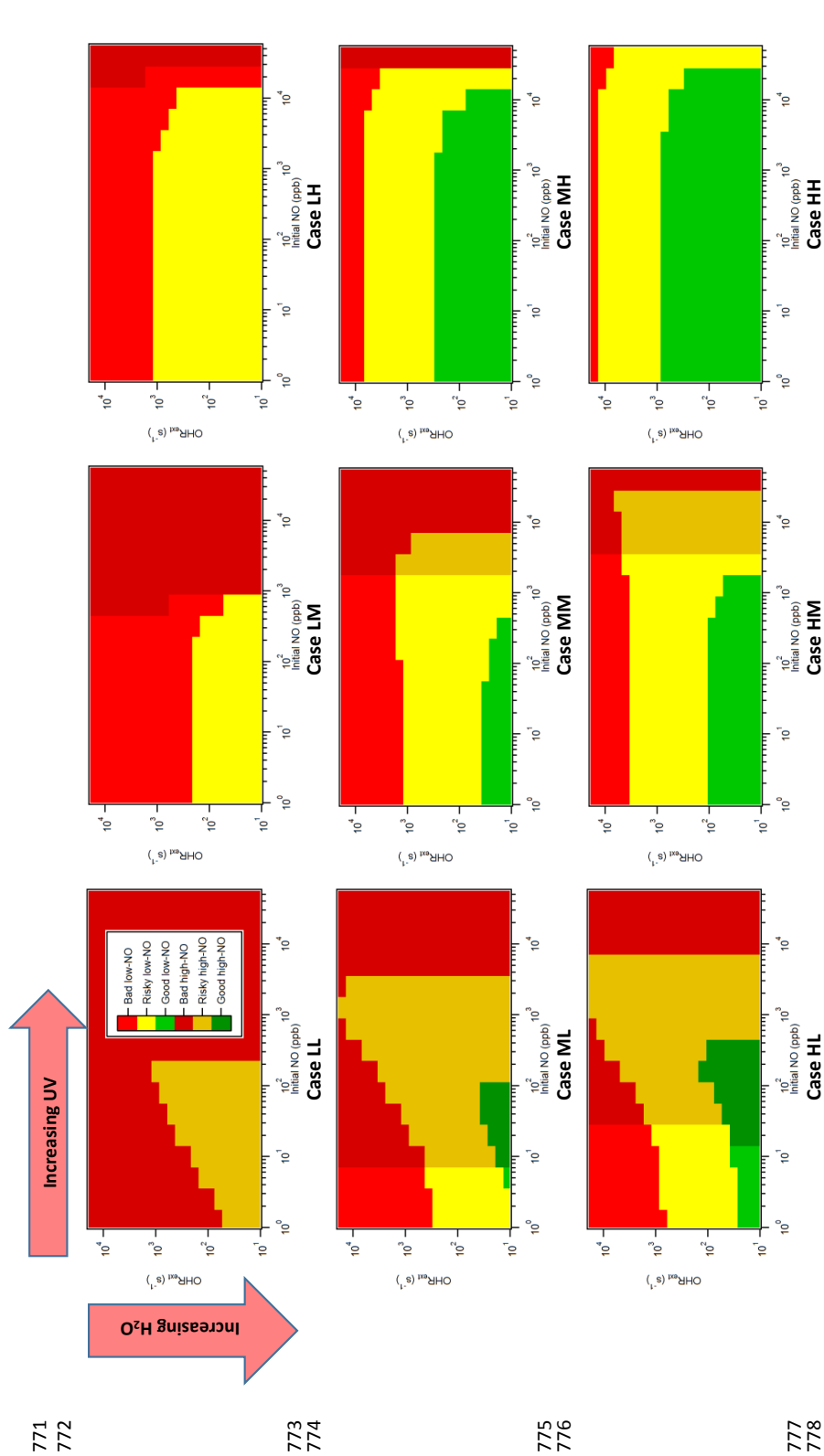
764

765

(b) OFR185-iNO

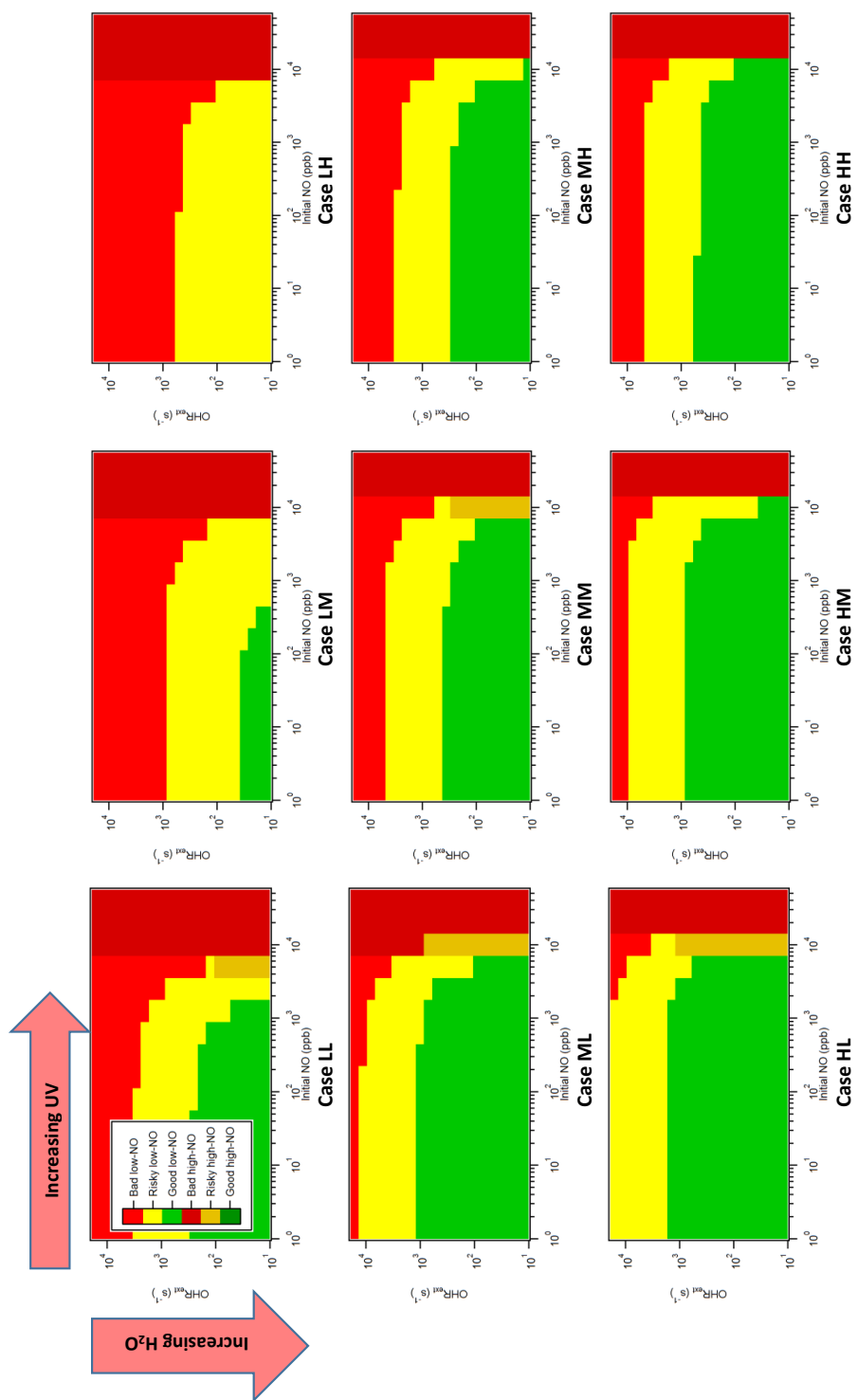
766 **Figure 3.** Frequency occurrence distributions of good, risky, and bad conditions (see Table 3) over  
767 logarithm of the ratio between RO<sub>2</sub> reacted with NO and with HO<sub>2</sub> (see Section S1 for more detail) for  
768 (a) OFR254-iNO (only the case with a residence time of 180 s) and (b) OFR185-iNO (including two cases  
769 with residence times of 180 and 30 s). Low and high-NO regions (see Table 3) are colored in light blue  
770 and grey, respectively.







779 **Figure 4.** Image plots of the condition types defined in Table 3 vs. external OH reactivity (excluding N-  
780 containing species) and initial NO for several typical cases in OFR185-iNO (see Table 2 for the case label  
781 code).  
782



783  
784

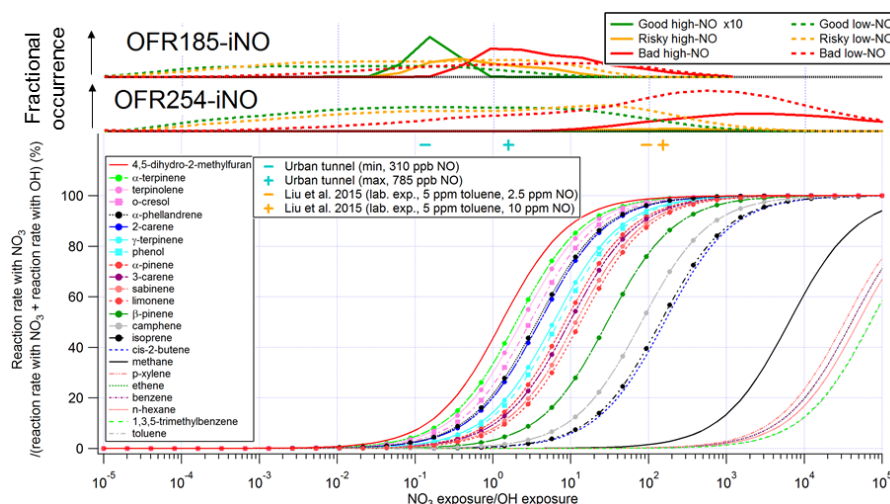
785  
786

787  
788

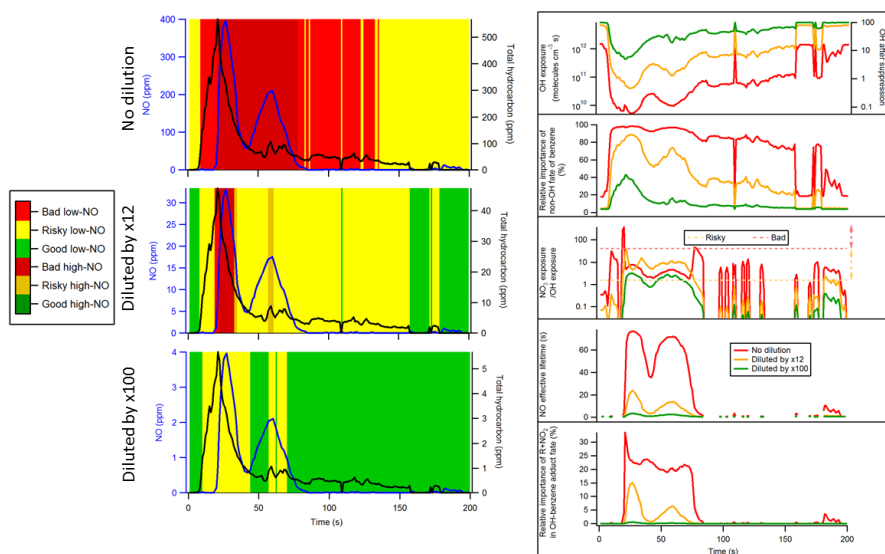
789  
790



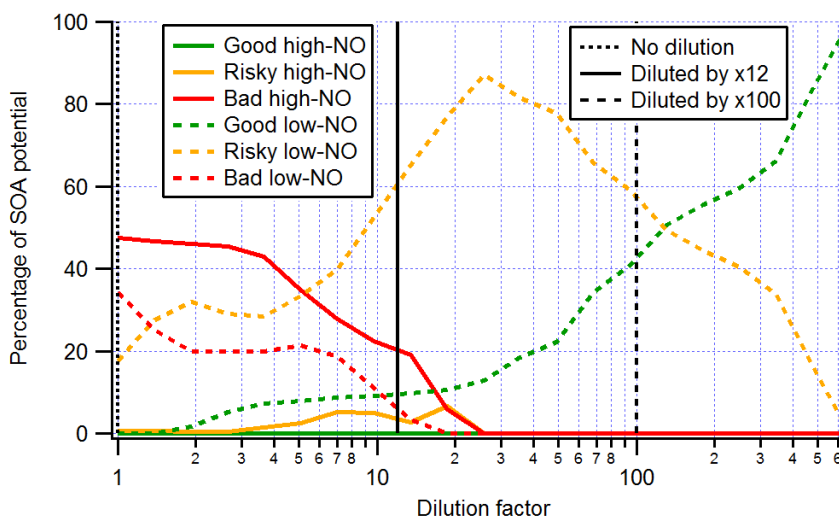
791 **Figure 5.** Same format as Fig. 4, but for OFR254-22-iNO.



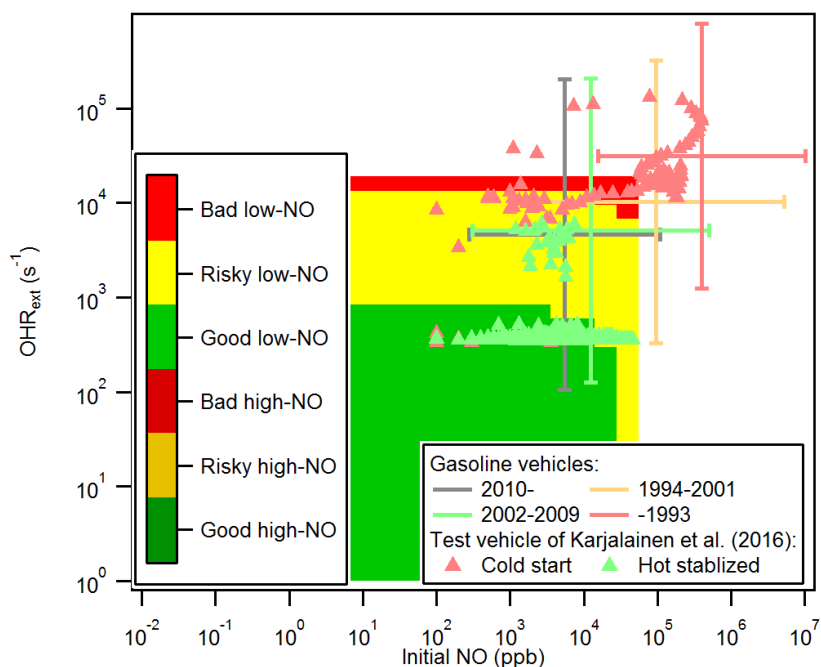
792  
 793 **Figure 6.** Fractional importance of the reaction rate of several species of interest with  $\text{NO}_3$  vs. that with  
 794 OH, as a function of the ratio of exposure to  $\text{NO}_3$  and OH. The curves of biogenics and phenols are  
 795 highlighted by solid dots and squares, respectively. The turquoise and orange markers show the ranges  
 796 of modeled exposure ratios between  $\text{NO}_3$  and OH of a source study in an urban tunnel (Tkacik et al.,  
 797 2014) and a laboratory study (Liu et al., 2015) using OFR, respectively. In the upper part of the figure,  
 798 the modeled frequency distributions of ratios of  $\text{NO}_3$  exposure to OH exposure under good/risky/bad  
 799 high/low-NO conditions for OFR185-iNO and OFR254-iNO are also shown. See Table 3 for the definitions  
 800 of the three types of conditions. All curves, and histograms in this figure share the same  
 801 abscissa.  
 802



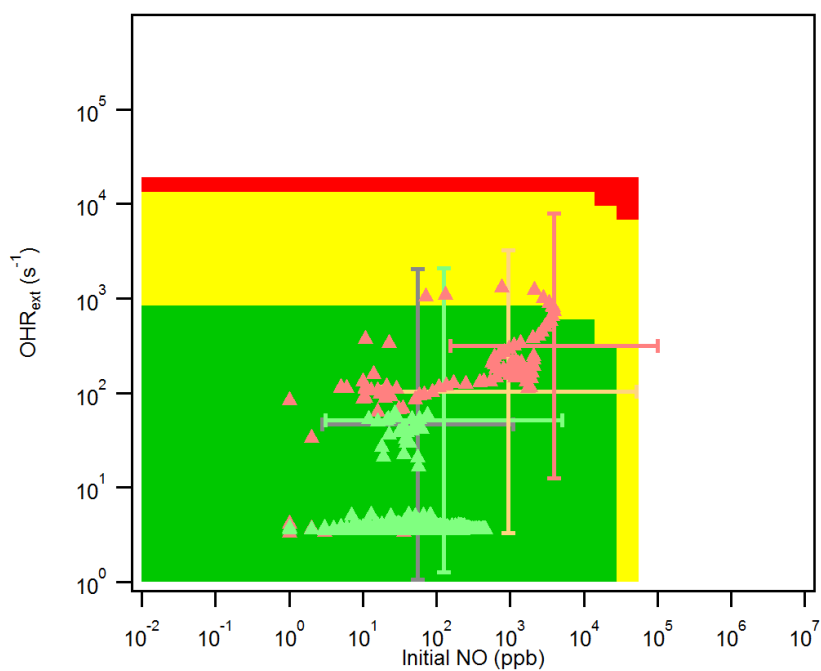
803  
804 **Figure 7.** (left) NO and total hydrocarbon during the first 200 s of the test of Karjalainen et al. (2016) in  
805 the cases of no dilution, dilution by a factor of 12 (as actually done in that study), and dilution by a  
806 factor of 100. Different periods of time are colored according to corresponding emissions (i.e., input  
807 conditions for OFR), classified as good/risky/bad high/low-NO. (right) OH exposure/percentage of  
808 remaining OH after suppression, relative importance of non-OH fate of benzene, exposure ratio of NO<sub>3</sub>  
809 to OH, NO effective lifetime, and relative importance of reaction of OH-toluene adduct with NO<sub>2</sub> in the  
810 fate of this adduct in the OFR of Karjalainen et al. (2016) during the first 200 s of their test in the cases  
811 of no dilution, dilution by a factor of 12, and dilution by a factor of 100. Horizontal orange and red  
812 dashed lines in the middle right panel denote “risky” and “bad” regions for exposure ratio of NO<sub>3</sub> to OH,  
813 respectively. Above the orange (red) dashed line, reaction with NO<sub>3</sub> contributes >20% to the fate of  
814 phenol (isoprene).



815  
816 **Figure 8.** Secondary organic aerosol (SOA) potential (estimated from the total hydrocarbon  
817 measurement) in the OFR of Karjalainen et al. (2016) formed during periods of time in the OFR  
818 corresponding to good/risky/bad high/low-NO conditions, as a function of dilution factor. Vertical lines  
819 denoting dilution factors of 1, 12 (as actually used in that study), and 100 are also shown.  
820

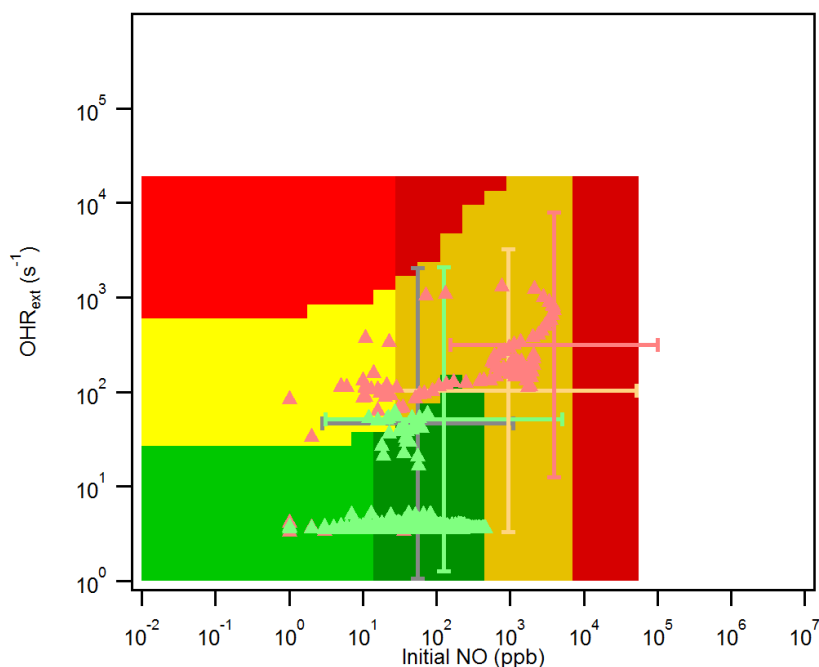


(a) No dilution (background: Case HH)



(b) Dilution by a factor of 100 (background: Case HH)





825

826

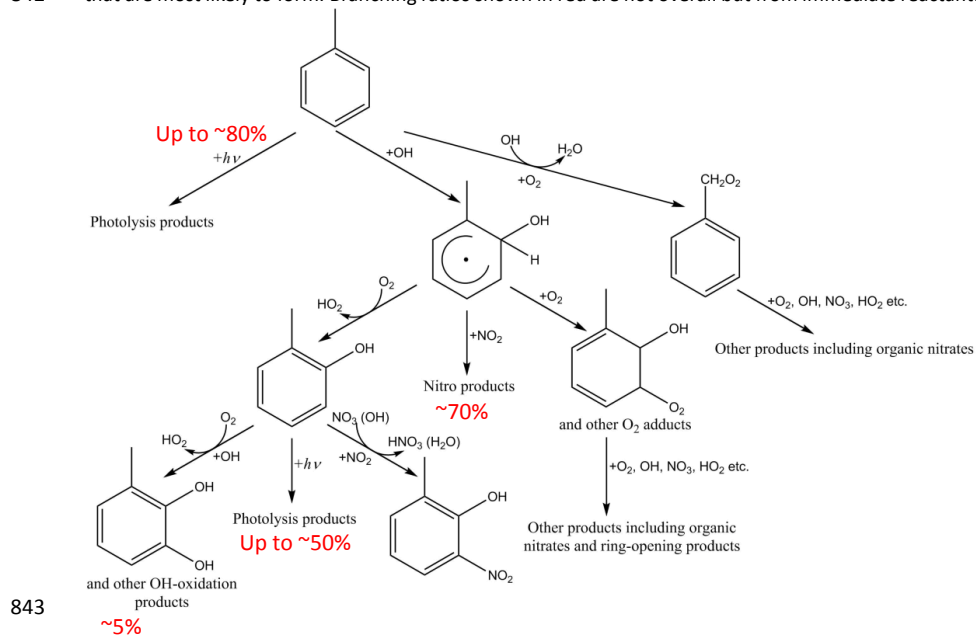
### (c) Dilution by a factor of 100 (background: Case HL)

827 **Figure 9.** Location of individual 1 s datapoints vs. OFR185-iNO reaction conditions. Datapoints are shown  
828 from the test vehicle of Karjalainen et al. (2016), as well as average exhaust from gasoline vehicle on-  
829 road emissions measured by Bishop and Stedman (2013). On-road emissions are classified by vehicle  
830 year and the distribution of each category is shown as a cross representing 1 standard deviation (with  
831 log-normal distribution assumed). The X and Y axes are NO and external OH reactivity (excluding N-  
832 containing species) due to vehicle emissions in OFR in the cases of (a) no dilution and (b,c) dilution by a  
833 factor of 100. The Karjalainen et al. (2016) points are classified as cold start (during first 200 s) and hot  
834 stabilized (during 200–1000 s). In addition, the same image plots as the panels of Cases HH (high H<sub>2</sub>O  
835 and high UV, see Table 2 for the case label code) and HL in Fig. 4 (OFR185-iNO) are shown as background  
836 for comparison.

837



838 **Scheme 1.** Possible major reactions in an OFR254-13-iNO with 5 ppm toluene and 10 ppm initial NO.  
839 Branching ratios in red are estimated by the model and/or according to Calvert et al. (2002), Atkinson  
840 and Arey (2003), Ziemann and Atkinson (2012), and Peng et al. (2016). Note that addition/substitution  
841 on the aromatic ring may occur at other positions. Intermediates/products shown here are the isomers  
842 that are most likely to form. Branching ratios shown in red are not overall but from immediate reactant.



844 **Table 1.** Experimental conditions of several OFR studies with high NO injection.

Study	Source type	Temperature (K)	Relative humidity (%)	Dilution factor	External OH reactivity of undiluted source (s <sup>-1</sup> )	Source NO <sub>x</sub> concentration (ppm)
Link et al. (2016)	Diesel vehicle emission		50	45–110	~5000 <sup>*1</sup>	436 <sup>*1</sup>
Martinsson et al. (2015)	Biomass burning emission			1700	156400 <sup>*1</sup>	154
Karjalainen et al. (2016)	Gasoline vehicle emission	295	60	12	~73000 <sup>*2,a</sup>	~400 <sup>*1,b</sup>
Liu et al. (2015)	Purified gas	293	13	1	~1400 <sup>*1,a</sup>	10 <sup>*1,b</sup>
Tkacik et al. (2014)	Tunnel air	293	42	1	~60 <sup>*1,a</sup>	~0.8 <sup>*1</sup>
Ortega et al. (2013)	Biomass burning emission	290	30	~500	~15-500	~0.2

845 <sup>\*1</sup> maximum value in the study846 <sup>\*2</sup> value at the moment of maximum NO emission847 <sup>\*a</sup> NO<sub>y</sub> species excluded848 <sup>\*b</sup> NO only

849



850 **Table 2.** Code of the labels of typical cases. A case label can be composed of four characters denoting  
 851 the water mixing ratio, the photon flux, the external OH reactivity excluding N-containing species, and  
 852 the initial NO mixing ratio, respectively. A case label can also be composed of two characters denoting  
 853 the water mixing ratio and the photon flux.

	Water mixing ratio	Photon flux	External OH reactivity (no ON)	Initial NO mixing ratio
Options	L=low (0.07%)	L=low ( $10^{11}$ photons $\text{cm}^{-2} \text{s}^{-1}$ at 185 nm; $4.2 \times 10^{13}$ photons $\text{cm}^{-2} \text{s}^{-1}$ at 254 nm)	0	0
	M=medium (1%)	M=medium ( $10^{13}$ photons $\text{cm}^{-2} \text{s}^{-1}$ at 185 nm; $1.4 \times 10^{15}$ photons $\text{cm}^{-2} \text{s}^{-1}$ at 254 nm)	L=low ( $10 \text{ s}^{-1}$ )	L=low (10 ppb)
	H=high (2.3%)	H=high ( $10^{14}$ photons $\text{cm}^{-2} \text{s}^{-1}$ at 185 nm; $8.5 \times 10^{15}$ photons $\text{cm}^{-2} \text{s}^{-1}$ at 254 nm)	H=high ( $100 \text{ s}^{-1}$ )	H=high (316 ppb)
			V=very high ( $1000 \text{ s}^{-1}$ )	V=very high (10 ppm)
Example	LHOV:	low water mixing ratio, high photon flux, no external OH reactivity (excluding ON), very high initial NO mixing ratio		
	ML:	medium water mixing ratio, low photon flux		

854

855

856 **Table 3.** Definition of condition types in this study (good/risky/bad high/low-NO).

Condition	Good	Risky	Bad
Criterion	$F_{185_{\text{exp}}}/OH_{\text{exp}} < 3 \times 10^3 \text{ cm s}^{-1}$ and $F_{254_{\text{exp}}}/OH_{\text{exp}} < 4 \times 10^5 \text{ cm s}^{-1}$	$F_{185_{\text{exp}}}/OH_{\text{exp}} < 1 \times 10^5 \text{ cm s}^{-1}$ and $F_{254_{\text{exp}}}/OH_{\text{exp}} < 1 \times 10^7 \text{ cm s}^{-1}$ (excluding good conditions)	$F_{185_{\text{exp}}}/OH_{\text{exp}} \geq 1 \times 10^5 \text{ cm s}^{-1}$ or $F_{254_{\text{exp}}}/OH_{\text{exp}} \geq 1 \times 10^7 \text{ cm s}^{-1}$
Condition	High-NO		Low-NO
Criterion*	$\frac{r(\text{RO}_2 + \text{NO})}{r(\text{RO}_2 + \text{HO}_2)} > 1$		$\frac{r(\text{RO}_2 + \text{NO})}{r(\text{RO}_2 + \text{HO}_2)} \leq 1$

857 \* See Section S1 for detail.